

T_{FH}-derived dopamine accelerates productive T:B synapses in human germinal centres

Ilenia Papa¹, David Saliba^{2§}, Maurilio Ponzoni^{3§}, Pablo F. Canete¹, Paula Gonzalez-Figueroa¹, Sonia Bustamante⁴, Salvatore Valvo², Michele Grimbaldston^{5,6}, Rebecca A. Sweet¹, Harpreet Vohra⁷, Michael Meyer-Hermann⁸, Michael L. Dustin², Claudio Doglioni^{3*} and Carola G. Vinuesa^{1,9*}.

¹*Department of Immunology and Infectious Disease, John Curtin School of Medical Research, Australian National University, Canberra, Australia.*

²*Kennedy Institute of Rheumatology, NDORMS, University of Oxford, Oxford, UK.*

³*Ateneo Vita-Salute, Department of Pathology, IRCCS Scientific Institute San Raffaele, Milan, Italy.*

⁴*Bioanalytical Mass Spectrometry Facility, Mark Wainwright Analytical Centre, UNSW, Sydney, Australia.*

⁵*Centre for Cancer Biology, University of South Australia and SA Pathology, Adelaide, Australia.*

⁶*OMNI-Biomarker Development, Genentech Inc, South San Francisco, California, USA.*

⁷*Imaging and Cytometry Facility, John Curtin School of Medical Research, Australian National University, Canberra, Australia.*

⁸*Department of Systems Immunology and Braunschweig Integrated Centre of Systems Biology, Helmholtz Centre for Infection Research, Braunschweig, Germany.*

⁹*China-Australia Centre for Personalised Immunology, Shanghai Renji Hospital, Shanghai Jiaotong University School of Medicine, Shanghai, China.*

* and §: Equal contribution

Correspondence: Carola G Vinuesa; carola.vinuesa@anu.edu.au

Protective high affinity antibody responses depend on competitive selection of B cells carrying somatically-mutated BCRs by T_{FH} cells in germinal centres (GC)^{1,2}. The rapid T:B synaptic interactions that occur during this process are reminiscent of those within the nervous system. Therefore, we asked whether neural transmission pathways participate in GC selection. Here we show that a proportion of human, but not mouse, GC T_{FH} cells contained dense-core granules marked by chromogranin B, which are normally found in neuronal pre-synaptic terminals and serve to store catecholamines such as dopamine^{3,4}. GC T_{FH} cells contained high concentrations of dopamine and released it upon cognate interaction with GC B cells. In a search for dopamine-mediated effects on human GC B cells, we identified selective and rapid upregulation of ICOSL. ICOSL-mediated costimulation has been shown to increase the contact area between GC B cells and T_{FH} cells, which maximises antigen presentation and delivery of T_{FH} cell help^{5,6}. In mice, upregulation of ICOSL by GC B cells is driven by T_{FH}-expressed CD40L in a process that takes hours⁶. In contrast, we show that ICOSL upregulation by human GC B cells did not depend on CD40L. High amount of intracellular preformed ICOSL was expressed in human GC B cells and translocated to the surface within minutes of stimulation by dopamine. ICOSL was able to enhance accumulation of CD40L and chromogranin B granules at the human T_{FH} cell synapse and increase the synapse area. Mathematical modelling suggests that faster dopamine-induced T:B interactions do not change affinity maturation but rather increase total output and accelerate it by days. Human T_{FH} cells have co-opted yet another form of synaptic help that may provide an evolutionary advantage in the face of infection.

Nervous and immune systems enable higher organisms to monitor their environments. Afferent signals register environmental cues that are usually processed by complex cell-cell interactions in the central nervous system, or secondary lymphoid organs, respectively. Lymphocytes co-opt elements of the molecular apparatus of neurons to form synapses that focus reception of antigen and costimulatory signals, and secretion of cytokines⁷. Within the immune system, B cells can take up, release and/or respond to catecholamines (CTs) (adrenaline, noradrenaline and dopamine)⁸⁻¹⁴ and human T cells have been reported to produce dopamine¹⁵. The generation of long-lived B cell effector responses takes place in germinal centres (GCs), where B cells and follicular helper T (T_{FH}) cells form multiple short-lived interactions in order to ensure efficient selection of rapidly-evolving

clones². When multiple B cell clones compete for limiting T cell help¹, signals that enhance T:B cell interactions are likely to increase or accelerate the chances of selection.

We stained human tonsil with a panel of antibodies against molecules involved in synaptic transmission, whose transcripts were previously shown to be upregulated in human T_{FH} cells¹⁶. Chromogranin B (CgB, encoded by *CHGB*), a protein that marks dense core neuroendocrine secretory granules containing catecholamines^{3,4}, showed positive and selective reactivity within T cells in GCs (Fig. 1a). We also found selective and high expression of *CHGB* RNA transcripts in T_{FH} cells by real time PCR and RNA-seq (Fig. 1b, c). CgB⁺ cells expressed all the markers associated with T_{FH} cells: CD3, PD-1, *ICOS*, CXCR5 and Bcl-6 (Fig. 1d and Fig. S1a); around 3-5% of all GC T cells stained positive for CgB (Fig. S1b, e). CgB⁺ cells were also found in human lymph node and spleen GCs (Fig. S1c-e). In mice, no CgB-expressing cells were detected in GC-rich secondary lymphoid tissues despite CgB⁺ cells being visible in neuroendocrine tissues, including pancreatic islets (Fig. S2a-g). *CHGB* transcripts were not detected either in mouse T cells (Fig. S2h). Although only a small subset of T_{FH} cells expressed CgB protein, when we analysed T_{FH} cells for *CHGB* transcripts using a live cell RNA detection probe, we detected high amounts of *CHGB* mRNA in the vast majority of GC-T_{FH} cells and intermediate amounts in pre-T_{FH} and other effector cells (Fig. 1e). This finding suggests that CgB protein can be rapidly regulated post-transcriptionally, rather than being confined to a subset of T_{FH} cells. We discovered increased CgB⁺ cell in IgG₄-related disease (IgG₄-RD, Fig. 1f, g) and three neoplasms of GC origin: T-Cell-Rich B-Cell Lymphoma (T/HRLBCL), nodular lymphocyte-predominant Hodgkin lymphoma (NLPHL)^{17,18} and angioimmunoblastic T cell lymphoma (AITL) (Fig. 1g). CgB⁺ cells were also visible in the ectopic GCs of Hashimoto's thyroiditis and were reduced in follicular lymphoma (FL) (Fig. 1g).

Electron microscopy of human GCs confirmed the presence of typical neurosecretory dense-core granules (Fig. 1h, i) that stained positive for CgB (Fig. 1j, k), and cytoplasmic CgB⁺ granules were visualised in sorted T_{FH} cells (Fig. 1l). These findings suggested that T_{FH} cells may contain catecholamines. We used highly specific tandem gas chromatography-mass spectrometry (GC/MS/MS) to quantify dopamine, adrenaline and noradrenaline (the three most abundant catecholamines in dense-core granules from presynaptic mammalian neurons) in sorted tonsil naïve T cells, T_{FH} cells and non-T_{FH} effectors (Fig. 2a). The only abundant catecholamine in T

cells was dopamine, which was found at high concentrations in T_{FH} cells and was barely detectable in the other T cell subsets (Fig. 2b). Flow cytometric staining using established protocols¹⁹ also revealed ~ 5% of T_{FH} cells contained dopamine ex vivo (Fig. 2c-e). Furthermore, incubation of purified T_{FH} cells with Forskolin (FSK), the cAMP-inducing agent reported to enhance dopamine synthesis¹⁹ increased the proportion of dopamine-containing T_{FH} cells by 4-fold (Fig. 2d, e). This was consistent with a detectable increase in transcription of chromogranin B (*CHGB*) and tyrosine hydroxylase (TH) (Fig. 2f), the enzyme responsible for catalysing the conversion of the amino acid L-tyrosine to L-3,4-dihydroxyphenylalanine (L-DOPA), the precursor for dopamine²⁰.

Having demonstrated that T_{FH} cells can store and synthesise dopamine, next we investigated the conditions that could trigger dopamine release. Whereas 30 minutes culture with anti-CD3/CD28 or with autologous GC B cells did not cause dopamine release, culture with allogeneic GC B cells to facilitate antigen-specific T_{FH}-B cell contacts caused over 50% reduction in dopamine (Fig. 2g), suggesting that cognate interactions with B cells are required to trigger dopamine release.

Analysis of expression of the dopamine receptors DRD1, 3 and 5 in human B cells²³ revealed abundant transcripts in GC and memory B cells (Fig. S3a). DRD1⁺ cells were enriched in GC light zones, some times in close proximity to CgB⁺ T cells (Fig. S3b, c). Dopamine augmented GC B cell differentiation to plasma cells induced by IL-21 (Fig. 2h, i). Specificity was confirmed by inhibition with the dopamine receptor antagonist haloperidol²⁴ (Fig. 2i). This effect was variable between different donors, with some donors exhibiting small or no effect (Fig. 2i). We did not detect any effect of dopamine on GC B cell proliferation, cell cycle kinetics or death (data not shown). Next, we investigated whether dopamine could regulate molecules important for GC B cell homeostasis or their ability to elicit T cell help. We could not see any effects of dopamine on surface expression of IL-21R, CD40, CD86, BAFFR, FAS or in intracellular BCL-6 (Fig. 3a). Strikingly, dopamine significantly upregulated surface ICOSL expression within 30 mins (Fig. 3a, b) without affecting GC B cell survival (Fig. 3c). The dopamine agonist SKF38393 also induced ICOSL upregulation in human GC B cells, an effect that was blocked by haloperidol and the more selective dopamine receptor 1 (DRD1) antagonist SKF83566 (Fig 3d). In contrast to the response observed in human GC B cells, dopamine did not induce ICOSL upregulation in mouse GC B cells (Fig. S4a).

143 This rapid dopamine-induced upregulation of ICOSL in GC B cells was reminiscent of
144 the rapid translocation to the surface of preformed CD40L upon activation of GC T_{FH}
145 cells²⁵. To investigate the possibility that pre-formed ICOSL is stored in human GC B
146 cells, we compared surface and intracellular ICOSL expression on the different
147 mouse and human B cell subsets. We found that human GC B cells expressed the
148 highest amounts of intracellular ICOSL (Fig. 3e, f). Mouse GC B cells also expressed
149 intracellular ICOSL (Fig. S4b). Consistent with post-transcriptional regulation, RNA-
150 sequencing did not reveal significant changes in *ICOSL* mRNA after two hours
151 incubation of GC and memory B cells with dopamine (Fig. 3g, Fig. S4c). Using a
152 selective blocker of protein synthesis/translation (cycloheximide, CHX), we also
153 showed that upregulation of ICOSL in human GC B cells in response to dopamine
154 did not require *de novo* protein synthesis (Fig. 3h). This treatment effectively blocked
155 ICOSL surface expression in mouse GC B cells (Fig. 3i). Together, these results
156 suggest that dopamine triggers rapid export of ICOSL from pre-formed stores to the
157 surface of human GC B cells.

158
159 T_{FH}-derived CD40L is the only signal known to-date to cause ICOSL upregulation in
160 mouse GC B cells⁶, an observation we replicated and found to occur at 4 hours but
161 not within 30 minutes (Fig. 3j). Intriguingly, whereas BAFF caused no ICOSL
162 modulation by 4 hours, LPS and anti-IgM stimulation, particularly at high dose,
163 induced ICOSL downregulation (Fig. 3j), suggesting functional compartmentalisation
164 of antigen/TLR and T cell-derived signals during GC B cell selection. As shown
165 previously for mouse B cells²⁶, CD40-mediated upregulation of ICOSL by mouse GC
166 B cells was dependent on transcription (Fig. S4d). Surprisingly, despite a broad
167 dose-range, CD40 signalling triggered by either an agonistic anti-CD40 antibody or
168 soluble CD40L did not induce ICOSL upregulation on human GC B cells within 30
169 min, 4h or 8h stimulation (Fig. 3k, l). CD40 ligation did increase human GC B cell
170 survival in these experiments as expected²⁷ (Fig. 3m). We investigated whether the
171 typical T_{FH}-derived cytokines might also be capable of inducing ICOSL expression by
172 human GC B cells within 30 minutes and found IL-21 to have some effect, albeit less
173 potent than DA, and no statistically-significant effect of IL-4 (Fig. 3n).

174
175 In mice, it has been shown that ICOSL on GC B cells engages ICOS on T_{FH} cells
176 leading to enhanced CD40 signalling⁶. To investigate if ICOSL can also increase
177 CD40L in activated human T cells, we used the *in vitro* supported lipid bilayer (SLB)
178 to precisely quantify the effects of ICOS ligation on CD40-dependent CD40L
179 accumulation at the synaptic cleft²⁸. Addition of ICOSL to the SLB increased the

amount of CD40L delivered to the synaptic cleft when CD40 was present in the SLB (Fig. 4a, b and Fig. S5a). When these experiments were performed using purified human T_{FH} cells, ICOS ligation increased the amount of CD40L delivered even in the absence of CD40 in the SLB (Fig. 4c). ICOSL also increased the ICAM-1⁺ synapse area (Fig. 4d, e), which is likely to contribute to the increased T:B cell entanglement reported in mice⁶. Most T_{FH} cells forming an immune synapse displayed chromogranin B signals within vesicle-like structures proximal to the synapse (Fig. 4f and Fig. S5b). As observed for CD40L, the abundance of chromogranin B signals proximal to the T_{FH} cell synapse also increased upon ICOS ligation (Fig. 4f, g). The presence of CgB⁺ granules in all Tfh cells forming synapses contrasts with the small fraction of CgB⁺ Tfh cells present within germinal centres (Fig. S1). It is therefore likely that cognate interactions with B cells and/or synapse formation rapidly promotes translation of the abundant *CHGB* mRNA present in all Tfh cells (Fig. 1b, c, e). Although granules marked by chromogranin B were not seen in mouse germinal centre cells, it is possible that mouse Tfh and /or GC B cells contain neurosecretory vesicles bearing other markers.

Together, our data suggest that human T_{FH} cells engaging in synaptic interactions with GC B cells can release dopamine stored in chromogranin B⁺ granules, which causes rapid translocation of B cell intracellular ICOSL to the surface. ICOS ligation increases the synapse area, causes translocation of CD40L to the T_{FH} cell surface and promotes further accumulation of chromogranin B granules rich in dopamine at the synapse. The resulting feed-forward loop would lead to sampling of a larger area of MHC-bound peptides by the TCR and to incremental increases in CD40L expression until the threshold for positive selection of the GC B cell is reached.

Our results demonstrated rapid dopamine-dependent ICOSL upregulation in human germinal centres but not in mice. As it is not possible to test the implications of fast versus slow ICOSL upregulation in experiments involving humans, we are forced to speculate about possible implications with the help of computer simulations. We started from the state-of-the-art mathematical model of GC reactions, validated with many experimental data²⁹⁻³¹, and explicitly included fast and slow up-regulation of ICOSL in GC-B cells (see supplementary material). Following the finding that T_{FH} signalling to B cells involves a positive feedback loop between ICOS and CD40 signalling (Fig. 4c and ⁶), we assumed that the level of ICOSL in the B cell modulates the amount of signals received from the T_{FH} cell. To our surprise, no impact on affinity maturation of GC B cells was found using fast or slow ICOSL upregulation in these

cells (Fig. 4h). However, a significant reduction and retardation of output production was found when ICOSL was upregulated slower (Fig. 4i). These results turned out robust against changes in the model assumptions and did not rely on the details of how B cells differentiated to output cells in the simulations (see supplementary material Figures S7-S9). In conclusion, the simulation results lead us to speculate that the dopamine-mediated improvement in the time required for B cells to elicit T cell help accelerates output of B cells from the GCs while keeping affinity maturation of GC B cells unchanged. This may provide an evolutionary advantage in the face of infection by rapidly evolving viruses and other infectious threats that have to be kept in check by high affinity antibodies.

Acknowledgments

We thank Prof. Jacopo Meldolesi for electron microscopy analysis interpretation and to Paola Podini for her technical assistance; Prof. Matt Cook and Dr Emmalene Bartlett for critical reading of the manuscript; Roberto Cairella for his contribution to the preparation of histological samples; Anastasia Wilson, Ann-Maree Hatch, Angel Lopez, and Emma Barry for assistance with obtaining tonsil samples and Di Yu for valuable suggestions. We thank the Imaging and Cytometry Facility and the Biomolecular Research Facility at the JCSMR for their technical support. CGV is supported by fellowship and grants from the Australian NHMRC. The Wellcome Trust supports MLD and SV and European Research Council grant AdG670930 supports MLD and DS. Human Frontier Science Program (RGP0033/2015) supports MMH, MLD, CGV.

Author contributions

I.P. performed most of the experiments and analysed the data. P.C., P.G. and H.V. helped with the experiments. M.P. contributed to data analysis. D.S. and S.V. performed SLB experiment and contributed to interpretation together with M.L.D. S.B. performed GC/GC/MS experiments. M.M-H. performed in silico modelling. M.G., M.L.D., M.M-H., M.P. and R.A.S. provided intellectual input, expertise and critical reading of the manuscript. I.P. and C.G.V. wrote the manuscript. C.G.V. supervised the project with D.C.

- 254 1 Victora, G. D. *et al.* Germinal center dynamics revealed by multiphoton
255 microscopy with a photoactivatable fluorescent reporter. *Cell* **143**, 592-605,
256 doi:10.1016/j.cell.2010.10.032 (2010).
- 257 2 Vinuesa, C. G., Linterman, M. A., Yu, D. & MacLennan, I. C. Follicular Helper
258 T Cells. *Annual review of immunology* **34**, 335-368, doi:10.1146/annurev-
259 immunol-041015-055605 (2016).
- 260 3 Malosio, M. L., Giordano, T., Laslop, A. & Meldolesi, J. Dense-core granules:
261 a specific hallmark of the neuronal/neurosecretory cell phenotype. *Journal of*
262 *cell science* **117**, 743-749, doi:10.1242/jcs.00934 (2004).
- 263 4 Schwarzenbrunner, U. *et al.* Sympathetic axons and nerve terminals: the
264 protein composition of small and large dense-core and of a third type of
265 vesicles. *Neuroscience* **37**, 819-827 (1990).
- 266 5 Shulman, Z. *et al.* Dynamic signaling by T follicular helper cells during
267 germinal center B cell selection. *Science* **345**, 1058-1062,
268 doi:10.1126/science.1257861 (2014).
- 269 6 Liu, D. *et al.* T-B-cell entanglement and ICOSL-driven feed-forward regulation
270 of germinal centre reaction. *Nature* **517**, 214-218, doi:10.1038/nature13803
271 (2015).
- 272 7 Wulfig, C. & Rupp, F. Neuropilin-1: another neuronal molecule in the
273 "immunological synapse". *Nature immunology* **3**, 418-419,
274 doi:10.1038/ni0502-418 (2002).
- 275 8 Kohm, A. P. & Sanders, V. M. Norepinephrine: a messenger from the brain to
276 the immune system. *Immunology today* **21**, 539-542 (2000).
- 277 9 McKenna, F. *et al.* Dopamine receptor expression on human T- and B-
278 lymphocytes, monocytes, neutrophils, eosinophils and NK cells: a flow
279 cytometric study. *Journal of neuroimmunology* **132**, 34-40 (2002).
- 280 10 Musso, N. R., Brenci, S., Setti, M., Indiveri, F. & Lotti, G. Catecholamine
281 content and in vitro catecholamine synthesis in peripheral human
282 lymphocytes. *The Journal of clinical endocrinology and metabolism* **81**, 3553-
283 3557, doi:10.1210/jcem.81.10.8855800 (1996).
- 284 11 Bergquist, J., Josefsson, E., Tarkowski, A., Ekman, R. & Ewing, A.
285 Measurements of catecholamine-mediated apoptosis of immunocompetent
286 cells by capillary electrophoresis. *Electrophoresis* **18**, 1760-1766,
287 doi:10.1002/elps.1150181009 (1997).
- 288 12 Bergquist, J. & Silberring, J. Identification of catecholamines in the immune
289 system by electrospray ionization mass spectrometry. *Rapid communications*
290 *in mass spectrometry : RCM* **12**, 683-688, doi:10.1002/(SICI)1097-
291 0231(19980615)12:11<683::AID-RCM218>3.0.CO;2-N (1998).
- 292 13 Musso, N. R., Brenci, S., Indiveri, F. & Lotti, G. Acetylcholine-induced,
293 calcium-dependent norepinephrine outflow from peripheral human
294 lymphocytes. *Journal of neuroimmunology* **87**, 82-87 (1998).
- 295 14 Marino, F. *et al.* Endogenous catecholamine synthesis, metabolism storage,
296 and uptake in human peripheral blood mononuclear cells. *Experimental*
297 *hematology* **27**, 489-495 (1999).
- 298 15 Cosentino, M. *et al.* Human CD4+CD25+ regulatory T cells selectively
299 express tyrosine hydroxylase and contain endogenous catecholamines
300 subserving an autocrine/paracrine inhibitory functional loop. *Blood* **109**, 632-
301 642, doi:10.1182/blood-2006-01-028423 (2007).
- 302 16 Chtanova, T. *et al.* T follicular helper cells express a distinctive transcriptional
303 profile, reflecting their role as non-Th1/Th2 effector cells that provide help for
304 B cells. *Journal of immunology* **173**, 68-78 (2004).
- 305 17 Brauninger, A. *et al.* Molecular analysis of single B cells from T-cell-rich B-cell
306 lymphoma shows the derivation of the tumor cells from mutating germinal

center B cells and exemplifies means by which immunoglobulin genes are modified in germinal center B cells. *Blood* **93**, 2679-2687 (1999).

18 Braeuninger, A. *et al.* Hodgkin and Reed-Sternberg cells in lymphocyte predominant Hodgkin disease represent clonal populations of germinal center-derived tumor B cells. *Proceedings of the National Academy of Sciences of the United States of America* **94**, 9337-9342 (1997).

19 Nakano, K. *et al.* Dopamine released by dendritic cells polarizes Th2 differentiation. *Int Immunol* **21**, 645-654, doi:10.1093/intimm/dxp033 (2009).

20 Daubner, S. C., Le, T. & Wang, S. Tyrosine hydroxylase and regulation of dopamine synthesis. *Archives of biochemistry and biophysics* **508**, 1-12, doi:10.1016/j.abb.2010.12.017 (2011).

21 Toppets, V. *et al.* Neuroimmune connections in ovine pharyngeal tonsil: potential site for prion neuroinvasion. *Cell and tissue research* **348**, 167-176, doi:10.1007/s00441-012-1376-x (2012).

22 Pfeil, U. *et al.* Intrinsic vascular dopamine - a key modulator of hypoxia-induced vasodilatation in splanchnic vessels. *The Journal of physiology* **592**, 1745-1756, doi:10.1113/jphysiol.2013.262626 (2014).

23 Meredith, E. J. *et al.* Dopamine targets cycling B cells independent of receptors/transporter for oxidative attack: Implications for non-Hodgkin's lymphoma. *Proceedings of the National Academy of Sciences of the United States of America* **103**, 13485-13490, doi:10.1073/pnas.0605993103 (2006).

24 Niemegeers, C. J. & Laduron, P. M. Pharmacology and biochemistry of haloperidol. *Proceedings of the Royal Society of Medicine* **69 suppl 1**, 3-8 (1976).

25 Casamayor-Palleja, M., Khan, M. & MacLennan, I. C. A subset of CD4+ memory T cells contains preformed CD40 ligand that is rapidly but transiently expressed on their surface after activation through the T cell receptor complex. *The Journal of experimental medicine* **181**, 1293-1301 (1995).

26 Watanabe, M. *et al.* Down-regulation of ICOS ligand by interaction with ICOS functions as a regulatory mechanism for immune responses. *Journal of immunology* **180**, 5222-5234 (2008).

27 Liu, Y. J. *et al.* Mechanism of antigen-driven selection in germinal centres. *Nature* **342**, 929-931, doi:10.1038/342929a0 (1989).

28 Choudhuri, K. *et al.* Polarized release of T-cell-receptor-enriched microvesicles at the immunological synapse. *Nature* **507**, 118-123, doi:10.1038/nature12951 (2014).

29 Meyer-Hermann, M. Overcoming the dichotomy of quantity and quality in antibody responses. *Journal of immunology* **193**, 5414-5419, doi:10.4049/jimmunol.1401828 (2014).

30 Meyer-Hermann, M. *et al.* A theory of germinal center B cell selection, division, and exit. *Cell reports* **2**, 162-174, doi:10.1016/j.celrep.2012.05.010 (2012).

31 Tas, J. M. *et al.* Visualizing antibody affinity maturation in germinal centers. *Science* **351**, 1048-1054, doi:10.1126/science.aad3439 (2016).

32 Meyer-Hermann, M., Deutsch, A. & Or-Guil, M. Recycling probability and dynamical properties of germinal center reactions. *J Theor Biol* **210**, 265-285, doi:10.1006/jtbi.2001.2297 (2001).

33 Dustin, M. L. & Meyer-Hermann, M. Immunology. Antigen feast or famine. *Science* **335**, 408-409, doi:10.1126/science.1218165 (2012).

Legend to Figures

Fig. 1. Human T_{FH} cells express chromogranin B and contain dense-core vesicles.

a, Immunohistochemistry showing chromogranin B (brown) expression in human GCs (dashed line) (n=50). Scale bar 100 μ m. **b**, qPCR and **(c)** RNA-sequencing showing high expression of *CHGB* mRNA in T_{FH} cells compared to other cell subsets extracted from three tonsils, expressed as relative unit (r.u.) or count per million (CPM). In qPCR experiments β 2-microglobulin was used as housekeeping gene. n=3. **d**, Immunofluorescence on human paraffin-embedded tonsil for CgB (red) and CD3, PD-1, CXCR5, ICOS and Bcl6 (green). Original magnification 400X (n=10). **e**, Flow cytometric plots showing *CHGB* mRNA detection probe in live CD3⁺ cells and MFI of the probe within the indicated cell subsets (n=5). **f**, Representative IHC stain of human lymph nodes from IgG₄-related disease. Scale bar 100 μ m (n=5). **g**, CgB⁺ cells per area in human reactive and neoplastic conditions. Bars represent medians and each dot represents the average of 10 areas from an individual patient. ns, not significant, (*p \leq 0.05), (**p \leq 0.01) nonparametric Mann-Whitney test (U test). **h**, **i**, EM showing ultrastructure of dense vesicles (arrows) within GC cells. ER=endoplasmic reticulum (n=3). **j**, **k**, Ultrathin LR white sections including cells that exhibit dense vesicles positive for CgB, labelled by immunogold particles. Immunolabelling is excluded from the negative cells at the bottom of panel k and from the extracellular space (ex.sp.) or spaces generated during processing (V). Scale bar 2 μ m (n=3). **l**, Immunofluorescence stain showing CgB⁺ granules in sorted T_{FH} cells (n=3).

Fig. 2. Human T_{FH} cells produce and release dopamine, which in turn enhances plasma cell differentiation in human GC B cells.

a, Gating strategy to isolate T_{FH}, T_{EFF} and T_{naive} cells from human tonsil by FACS sorting. **b**, Quantification of L-DOPA, dopamine, noradrenaline and adrenaline in the indicated cell subsets by GC/MS/MS. Values are expressed in fmol/10⁶ cells. Cells have been sorted and pooled together from three donors (n=2). **c**, Quantification of DA-expressing cells in the indicated cell subsets by flow cytometric and immunofluorescence analysis (n=3). **d**, Representative immunofluorescence images for dopamine of ex-vivo and forskolin treated T_{FH} cells (n=5). **e**, Quantification of DA-expressing T_{FH} cells before and after 24 h treatment with Forskolin (FSK). Bars represent median values and each dot represents a donor (n=5). (**p \leq 0.01)

nonparametric Mann-Whitney test (U test). **f**, qPCR showing upregulation of *TH* and *CHGB* mRNA in T_{FH} cells after Forskolin treatment. r.u., relative unit. *RPL13A* was used as housekeeping gene. Bars represent median values and each dot represents a donor (n=3). (* $p \leq 0.05$), (** $p \leq 0.01$) nonparametric Mann-Whitney test (U test). **g**, Bar plot showing dopamine release from T_{FH} cells after 30 min stimulation with anti-CD3/CD28 beads (1:1), autologous and allogeneic GC B cells (1:2). T_{FH} cells were pre-stimulated with forskolin before inducing DA release. Bars represent median and each dot represent a single experiment conducted in triplicates (n=3). ns, not significant, (* $p \leq 0.05$) nonparametric Mann-Whitney test (U test). **h**, Flow cytometric plots showing plasma cells, identified as $CD27^{hi}CD38^{hi}$, induced in cultures of GC B cells stimulated for five days with anti-CD40 (2 μ g/ml), IL-21 (20 ng/ml) and different concentrations of freshly made DA (n=5). **i**, Fold changes in plasma cell (PC) differentiation from GC B cells stimulated for 2h with or without DA (5 μ M) and Haloperidol (50nM), and cultured in the presence of anti-CD40 (2 μ g/ml) and IL-21 (20 ng/ml) for five days. Bars represent median and each dot represent a single experiment conducted in triplicates (n=5). (* $p \leq 0.05$) two tailed student t-test.

Fig. 3. Dopamine induces ICOSL upregulation on human GC B cell without requiring transcription or de novo protein synthesis.

a, Gate for identifying GC B cells and representative histogram of specified surface markers after 30 minutes of stimulation with or without DA (10 μ M) (n=3). **b**, Fold changes of surface ICOSL expression on GC B cells that were stimulated with DA (10 μ M) for 30 min, with medium control set as unit 1. Bars represent median values and each dot represents a separate experiment conducted in triplicate (n=8). (*** $p \leq 0.001$) two tailed student t-test. **c**, Bar plot showing survival of GC B cells in DA stimulation experiments (n=8). **d**, Fold changes of surface ICOSL expression on GC B cells that were stimulated with DA (10 μ M), SKF38393 (10nM), Haloperidol (50nM) and SKF83566 (10nM) for 30 min, with medium control set as unit 1. Bars represent median values and each dot represents a separate experiment conducted in triplicate (n=5). (* $p \leq 0.05$), (** $p \leq 0.01$) two tailed student t-test. **e**, **f**, Representative histogram and quantification of surface and intracellular ICOSL on naïve, memory and GC B cells (n=4). (** $p \leq 0.01$), (*** $p \leq 0.001$) and (**** $p \leq 0.0001$) nonparametric Mann-Whitney test (U test). **g**, RNA counts per million (CPM) of indicated transcripts in human GC B cells stimulated with or without DA (5 μ M) for 2h (n=3). **h**, Fold changes of surface ICOSL expression on human GC B cells that were treated with cycloheximide (CHX, 10 μ g/ml) and stimulated with DA (10 μ M) for 30 min, with

medium control set as unit 1. Bars represent median and each dot represent a single experiment conducted in triplicates. ($^{***}p \leq 0.001$) two tailed student t-test. **i**, Fold changes of surface ICOSL expression on mouse GC B cells that were treated with cycloheximide (CHX, 10 $\mu\text{g/ml}$) for 4h, with medium control set as unit 1. Bars represent median values and each dot represents a single mouse. ($^{***}p \leq 0.001$) two tailed student t-test. **j**, Fold changes of surface ICOSL expression on mouse GC B cells that were stimulated with BAFF (100ng/ml), LPS (1 or 10 $\mu\text{g/ml}$), anti-CD40 (10 $\mu\text{g/ml}$) and anti-IgM (1 or 10 $\mu\text{g/ml}$) for 30 min and 4h. Unit 1 set on medium control. ns, not significant, ($^*p \leq 0.05$), ($^{***}p \leq 0.001$) and ($^{****}p \leq 0.0001$) two tailed student t-test. **k**, Representative histogram and fold changes of surface ICOSL expression on human GC B cells that were stimulated with DA (10 μM), anti-CD40 (1 $\mu\text{g/ml}$) or recombinant CD40L (10 $\mu\text{g/ml}$) for 30 min with medium control set as unit 1. Bars represent median values and each dot represents a single experiment conducted in triplicate. ($^{**}p \leq 0.01$) and ($^{***}p \leq 0.001$) two tailed student t-test. (n=5). **l**, Fold changes of surface ICOSL expression on human GC B cells stimulated with several concentrations of anti-CD40 for 4 and 8 hours, with medium control set as unit 1 (n=3). **m**, Bar plot showing survival of GC B in the presence of anti-CD40 (1 $\mu\text{g/ml}$) after 4 or 8 hours of stimulation (n=4). **n**, Representative histogram and fold changes of surface ICOSL expression on human GC B cells that were stimulated with DA (10 μM), IL-21 (10, 50 or 100 ng/ml) or IL-4 (10 ng/ml) for 30 min, with medium control set as unit 1. Bars represent medians and each dot represents a single experiment conducted in triplicates (n=10). ns, not significant, ($^{**}p \leq 0.01$), ($^{***}p \leq 0.001$) and ($^{****}p \leq 0.0001$) two tailed student t-test.

Fig. 4. Modelling of DA effect on T_{FH} cell-GC B cell communication and germinal centre output

a, Supported lipid bilayer (SLB) model for T cell-B cell communication. SLB containing ICAM-1, UCHT1 with or without CD40 and ICOSL to model effect of DA dependent ICOSL expression by GC B cells on reception of CD40L. Representative images of ICAM-1 ring (white) around CD40L (pseudocolor scale) in the presence of absence of CD40 and ICOSL at physiological densities. Scale bar 5 μm . **b**, **c**, Plots represent CD40L fluorescent intensity of individual activated human T (**b**) or T_{FH} (**c**) cells forming synapses (n=3). ns, not significant, ($^{***}p \leq 0.001$) and ($^{****}p \leq 0.0001$) nonparametric Mann-Whitney test (U test). **d**, Representative ICAM-1 area quantification. **e**, Tukey box plot representation of ICAM-1 area, expressed as relative unit (r.u.). ($^{***}p \leq 0.001$) nonparametric Mann-Whitney test (U test). **f**,

466 Representative images of chromogranin B stain in the presence of absence of
 467 ICOSL at the immunological synapse. **g**, Plots represent CgB fluorescent intensity of
 468 individual activated T_{FH} and non- T_{FH} cells forming synapses ($n=3$). (**** $p \leq 0.0001$)
 469 nonparametric Mann-Whitney test (U test). **h, i**, The impact of the speed of ICOSL
 470 upregulation Δt_{ICOSL} in GC-B cells onto GC characteristics (mean affinity (**h**) and
 471 produced output (**i**)) was estimated with computer simulations. Fast (black and grey
 472 lines) and slow (colored lines) ICOSL upregulation are compared. The comparison
 473 was repeated for simulations with short (black, red, orange lines) and long (grey,
 474 magenta, cyan lines) periods of search for T_{FH} cells. Ω is a simulation read-out that
 475 reflects the strength of the GC reaction. Slow ICOSL upregulation had the tendency
 476 to shrink GCs (small Ω , red and magenta lines). In order to exclude that less output
 477 simply reflects smaller GCs, the GC strength was restored by variation of two
 478 parameters: The duration $\Delta t_{T_{fh}}$ (given in hours per successful antigen collection event
 479 from FDCs) of the period during which B cells search for signals from T_{FH} and the
 480 amount of integrated T_{FH} -signals $S(N_p=2)$ required to induce 2 divisions of the B cell
 481 after recycling. Lines are the mean of 100 simulations, grey shades show the
 482 standard deviations (See supplementary material for more details).

Legends to Supplementary Figures

Fig. S1. CgB⁺ cells in human GC.

a, Representative immunofluorescence images for CD3 (green) and ICOS (red) in human germinal centres. **b**, Representative double immunohistochemistry for CgB (left) and CD3 (middle) after colour deconvolution. Pseudo-colour image (right) showing signal colocalisation. Original magnification 40X. Scale bar 100 μ m (n=3). **b**, **c**, Representative immunohistochemistry for CgB (brown) of human lymph node (**b**) and spleen (**c**). (n=10). **e**, Quantification of CD3⁺CgB⁺ cells in human tonsils, lymph nodes (n=10) and spleens (n=5). ns, not significant, (*p \leq 0.05) nonparametric Mann-Whitney test (U test).

Fig. S2. Mouse chromogranin B expression.

a-c, Hematoxylin/Eosin staining of three different mouse spleen GCs. **d-f**, IHC staining shows no CgB reactivity in the same GCs. **g**, IHC control staining for CgB in mouse pancreas islets. (**a-g**) Original magnification 60X. Scale bar 100 μ m. n=3 **h**, Relative mouse *CHGB* mRNA expression in different T cell subsets with adrenal gland as positive control. T cells were FACS sorted as follows: T_{naïve} (CD4⁺ CD44^{lo} CD25⁻); T effector memory (T_{EM}, CD4⁺ CD44^{hi} CD25⁻ PD-1^{-/lo} CXCR5^{-/lo}); T_{FH} (CD4⁺ CD44^{hi} PD-1^{hi} CXCR5^{hi}); T_{REG} (CD4⁺ CD25⁺ CD44^{int}). *GAPDH* was used as housekeeping gene (n=3).

Fig. S3. Dopamine receptors (DRDs) expression in human B cell subsets.

a, relative expression of DRDs mRNA in human B cell subsets normalised to naïve B cells. β 2-microglobulin was used as housekeeping gene (n=3). Error bars show s.d. **b**, **c**, Representative images of dopamine receptor 1⁺ cells (green) localisation in human GC (dashed line), showing close proximity to CgB⁺ (**b**) or CD3⁺ (**c**) cells (red) (n=3).

Fig. S4. Regulation of ICOSL upregulation in mouse and human B cells

a, Fold changes of surface ICOSL expression on mouse GC B cells that were treated with anti-CD40 (10 μ g/ml) and DA (0.5, 1, 5, 10 μ M) for 30 minutes, with medium control set as unit 1 (n=5). **b**, Representative histogram and quantification of surface and intracellular ICOSL on GC and non-GC B cells (n=5). (**p \leq 0.01) nonparametric Mann-Whitney test (U test). **c**, RNA counts per million of ICOSL, CD40, BCL6, IL21R, CD86, BAFFR and FAS mRNA in human memory B cells stimulated with or

without DA (5 μ M) for 2h (n=3). **d**, Fold changes of surface ICOSL expression on mouse GC B cells that were treated with actinomycin D (ActD, 5 μ g/ml), anti-CD40 (10 μ g/ml) for 4h, with medium control set as unit 1. Bars represent median and each dot represent a single mouse (n=5). (** $p \leq 0.01$) and (***) $p \leq 0.001$) two tailed student t-test.

Fig. S5. Effect of ICOSL on CD40L presentation and reception in SLB model for T_{FH} cell- GC B cell interaction.

a, Activated human T cells that express ICOS and CD40L were incubated with SLB containing ICAM-1 and UCHT1 (anti-CD3) as a basal condition with a ring of ICAM-1 surrounding a central cluster enriched in T cell receptor enriched extracellular vesicles by 15 minutes²⁸. This condition resulted in low presentation of CD40L in punctate structures detected by anti-CD40L mAb that accumulated in the same central synapse with the TCR enriched extracellular vesicles. Addition of ICOSL the SLB resulted in strong central accumulation of fluorescent ICOSL with the TCR enriched extracellular vesicles, but no increase in CD40L presentation. Addition of CD40 the SLB resulted in a significant increase in CD40L accumulation, which we refer to as reception because its receptor dependent. When ICOSL and CD40 were added the reception of CD40L was further significantly enhanced over the level observed with CD40 alone. Thus, ICOSL ligation in the centre of the immunological synapse increases CD40L reception. All levels are shown in gray scale except CD40L panels, for which the pseudocolor scale is indicated. Scale bar = 5 μ m. **b**, Human T_{FH} cells were incubated with SLB containing ICAM-1 and UCHT1 (anti-CD3). Addition of ICOSL resulted in increased accumulation of CgB at the synapse centre. Addition of CD40 did not further increased CgB accumulation.

Fig. S6. Dopamine derivative structure.

Diagram showing chemical structure of dopamine derivative after sample reconstitution with trifluoroacetic anhydride (TFAA) and trifluoroethanol (TFE).

Fig. S7. Effect of ICOSL upregulation speed in the published GC LEDA model.

Characteristics of GC reactions in simulations with short (black) and long (colours) search phase for T_{FH} help using the previously published LEDA model (see text). All tested variants (see legend box and text for details on the quantities) exhibit reduced and retarded output production while keeping affinity maturation unchanged. Mean (full lines) and standard deviation (shades) of 100 simulations.

Fig. S8. Effect of ICOSL upregulation speed in the extended LEDA model of GCs.

The LEDA model in Figure S7 was extended to allow for multiple short contacts between B and T cells and to explicitly represent ICOSL dynamics in B cells (see text for details). Characteristics of GC reactions in simulations with fast (black, grey) and slow (colours) ICOSL upregulation. All tested variants (see legend box and text for details on the quantities) exhibit reduced and retarded output production while keeping GC B cell affinity unchanged. Output affinity is enhanced in a subset of settings. Mean (full lines) and standard deviation (shades) of 100 simulations.

Fig. S9. Effect of ICOSL upregulation speed in the classical recycling model.

The simulations in Figure S8 were repeated using the classical textbook recycling model with 80% of the selected B cells doing recycling and 20% of the selected B cells differentiating to output cells³². This replaced the LEDA model in Figures S2. The simulations with short search periods for T_{FH} help were repeated. Note that the overall output production is smaller in the classical recycling model³³. The relative reduction of output in simulations with slow ICOSL upregulation is unchanged. Mean (full lines) and standard deviation (shades) of 100 simulations.

Table S1. List of Selected Reaction Monitoring for Catecholamines under study

Online Materials and Methods

Human tonsil and lymphoid tissues

Human tonsils were obtained from children undergoing routine tonsillectomy at The Canberra Hospital and Calvary John James Hospital. A single cell suspension was obtained by mechanical disruption of the tissue followed by cell separation using Ficoll Hypaque (GE Healthcare Life Sciences) gradient. Informed consent was obtained from all subjects. All experiments with human samples were approved by the Australian National University's Human Experimentation Ethics Committee and the University Hospitals Institutional Review Board. All tissue samples used for histology were retrieved from the paraffin and cryopreserved archives of the Pathology Unit of San Raffaele Scientific Institute and utilized following IRB-approved institutional rules.

Mice, immunizations and spleen cell suspensions

C57BL/6 (B6) mice were bred and maintained in specific-pathogen-free conditions at the Australian Phenomics Facility, ANU. All procedures carried out were approved by the Australian National University's Animal and Human Experimentation Ethics Committees. To generate thymus-dependent GC responses, mice were immunized i.v. with 2×10^8 SRBCs (Applied Biological Products Management, Australia) and were taken down at day 7 post immunization. Single-splenocyte cell suspensions were prepared by mechanically disrupting the tissue through 70 μ m nylon mesh filters (BD Bioscience) in complete RPMI 1640 media (Sigma). For RNA analysis T cell subsets were isolated using FACS sorting following surface staining with CD4 FITC (RM4-5, BioLegend), CD44 Alexa Fluor 700 (IM7, BioLegend), CD25 APC (PC61, BD Pharmingen), CXCR5 biotin (2G8, BD Pharmingen), PD-1 Brilliant Violet 421 (29F.1A12, BioLegend), Streptavidin PE-Cy7 (BioLegend) and 7-AAD (Invitrogen). For ICOSL induction experiments, B cells were isolated using MACS columns (Miltenyi Biotec) according to the manufacturer's instructions. 5×10^5 cells were stimulated with BAFF (100 ng/ml, R&D), lipopolysaccharides (LPS, 1 or 10 μ g/ml, Sigma) from E. coli, anti-CD40 (10 μ g/ml, BioXCell), anti-IgM (1 or 10 μ g/ml, Jackson ImmunoResearch Laboratories) and indicated concentration of DA (Sigma) for 30 min or 4 h. Cells were stained for Zombie Aqua fixable viability kit (BioLegend), B220 (RA3-6B2, BD Pharmingen), GL-7 (GL7, BioLegend). Fas (Jo2, BD Pharmingen), CD3 (17A2, BD Pharmingen), ICOSL (HK5.3, BioLegend). Intracellular

staining for ICOSL was performed using the FOXP3/Transcription Factor Staining Buffer Set (eBioscience) according to the manufacturer's instructions.

Immunohistochemistry

Using immunohistochemistry technique, the presence and location of CgB positive cells were evaluated in a series of non-neoplastic lymphoid tissues, from different anatomical sites including tonsils (n=50), lymph-nodes (n=10) and spleens (n=10). Immunohistochemistry was also performed on pancreas and spleens of SRBC immunized mice (n=3). Heat-induced antigen retrieval in Tris EDTA buffer (pH 9.0) for 30 min at 97 °C was used, followed by blocking of endogenous peroxidase with 3% H₂O₂ and incubation with 3% normal bovine serum. Primary antibody against CgB (H300, Santa Cruz) was incubated for 1 h at room temperature, followed by detection with HRP conjugate-polymer (Thermo Scientific, Fremont, CA, USA) and developed with DAB chromogen. Selected samples underwent also double immunohistochemistry technique to evaluate simultaneous expression of CD3 (LN10, Dako) with CgB. Stained slides, underwent a second round of blocking in Tris EDTA buffer (pH 9.0), overnight incubation with the second primary antibody at 4°C and developed using AP conjugate-polymer and Fast Red chromogen (Thermo Scientific, Fremont, CA, USA). Tissue sections were counterstained with haematoxylin and scanned with Aperio ScanScope. Selected areas were analyzed with Aperio Color Deconvolution v9 algorithm and then, to produce multicolor composite images, digital snapshots were individually pseudocolored and overlaid in Adobe Photoshop CS3 (Adobe Systems, Inc., San Jose, CA)¹.

To establish the number of CgB positive cell in different reactive, autoimmune and neoplastic conditions, immunohistochemistry CgB was performed on paraffin-embedded sections of reactive lymph-node/tonsil, T cell rich/histiocytic B cell Lymphoma (THRLBCL), Nodular Lymphocyte Predominant Hodgkin Disease (NLPHL), Angioimmunoblastic-like T-cell lymphoma (AITL), Hashimoto's thyroiditis, IgG₄-related disease (IgG₄-RD) and Follicular Lymphoma (FL) (n=5). Slides were digitally scanned using Aperio ScanScope software and 10 GCs for each sample were manually selected and analyzed for chromogranin B expression. CgB⁺ cells were counted in 10 selected areas for each sample. The results were expressed as the number of CgB⁺ cells per area.

Immunofluorescence

Frozen tonsil sections were fixed in cold 4% PFA for 20 min and blocked using 3% BSA. Heat-induced antigen retrieval in Tris EDTA buffer (pH 9.0) for 30 min at 97°C was used to retrieve antigens on paraffin-embedded tonsil samples. Sections were then stained using CD3 (LN10 or polyclonal, Dako), PD-1 (NAT105, CNIO, Madrid), CXCR5 (51505, R&D), ICOS (AF169, R&D), BCL6 (LN22, Novocastra), CgB (H300, Santa Cruz), DRD1 (L205G1, BioLegend) for 1h at RT in the dark, followed by anti-mouse Alexa Fluor 488 (A-21202, Invitrogen) and anti-rabbit Alexa Fluor 594 (A-21207, Invitrogen) for 30 min at RT in the dark. Stained sections were mounted using Vectashield with DAPI mounting media (Vector Laboratories, #H-1200). Images were collected with an Olympus IX71 microscope with DP Controller software (Olympus) and compiled by using ImageJ software.

Electron microscopy

Five samples of human reactive tonsil were prepared and analyzed with LEO 912AB (LEO Electron Microscopy Ltd. Cambridge, UK) electron microscope. In order to confirm the localization of CgB in dense core vesicles human reactive tonsils ($n=3$) were analyzed by immunoelectron microscopy², using an anti-CgB pAb (H300, Santa Cruz).

Gas Chromatography-Mass Spectrometry

T follicular helper cells, naïve and non- T_{FH} effector cells were isolated and pooled from human tonsils and were extracted using an ice-cold solution of 5M formic acid in n-butanol (1:4) and frozen till further analysis. Dopamine, noradrenaline, adrenaline and L-DOPA were measured by a highly specific Gas Chromatography Tandem Mass spectrometry (GC/MS/MS) assay. Catecholamine extraction and derivatization procedures previously described³ were slightly modified to determine Adrenaline, noradrenaline, dopamine and DOPA (no internal standards were used to ensure that no significant deuterium exchange contribution occurred during sample preparation considering expected low endogenous levels). Standards were prepared in 0.05M aqueous formic acid and calibrators were prepared within the 0.5-500 nM range. Standards and cell extracts were transferred to 13x100 mm glass culture tubes, dried and reconstituted in 2ml Tris buffer (pH 8.6) before adding a scoop (~200mg) of acid activated alumina and shaken gently for 15 min. After alumina settled, supernatant buffer was aspirated to waste and 5-6 water washes were made (aspirated and discarded) to reach neat water pH. The aqueous alumina slurry containing adsorbed catecholamines was transferred to glass Pasteur pipettes with silanized glass wool plugs. Packed alumina was rinsed with 1ml of water and then with 0.5 ml of 50%

methanol. Catecholamines were carefully and slowly desorbed with 400 μ L elution solvent (methanol:water:formic acid in the ratio of 6:1:0.25, pH3) into clean screw cap glass culture tubes. Alumina was flushed twice (2x400 μ L) with eluting solvent to complete recovery. The contents were dried down under vacuum using a SpeedVac, (Thermo Scientific, Asheville, NC, USA). The dried samples were reconstituted using 80 μ L of trifluoroethanol (TFE), 40 μ L of trifluoroacetic anhydride (TFAA) and 30 μ L of toluene. Tubes were capped and heated at 75°C for 30 min. Derivatives (Dopamine derivative, Fig. S6) were transferred to glass vials and four μ L were then injected into the GC. Selected reaction monitoring (SRM) transitions used in this method were evaluated for each individual trifluoroacetyl derivative and instrument conditions were optimized to ensure maximum sensitivity, collision energy was set at 20V for all transitions monitored. Analysis was performed using a Trace GC Ultra interfaced with a TSQ XLS Mass Spectrometry Detector and a Triplus autosampler (Thermo Scientific, San Jose, CA), operated in electron capture negative ionization (ECNI) mode. Methane and argon were used as the ECNI reagent and collision gas, respectively. Chromatographic separation was carried out using an Agilent 30 metre HP-5MS (0.25 mm ID \times 0.25 μ m film thickness) column. Helium was used as a carrier gas with flow rates of 1.2 mL/min. Argon flow in the collision cell was 1.0 mL/min. Four μ L injection volumes were made at 250°C in splitless mode. The oven temperature program was as follows: 90°C for 0.5 min, 20°C/min to 160°C, held 2 min; then 5°C/min to 170°C. The temperature was again increased to 280°C at 20°C/min. The temperature of the CI source and of the quadrupoles (Q1 and Q3) was 200°C and the auxiliary MS transfer line 275°C. The ECNI reagent gas flow was set at 2.0 mL/min. SRM transitions for each analyte are listed in Table S1. Data analysis was performed using XcaliburTM software (Thermo Scientific, San Jose, CA). The quantification method detailed all compound information, which included expected peaks and their target signals as well as their expected retention times. Standard samples were tagged and the integration results (peak areas vs. concentration) were used to determine a linear regression curve for each analyte. These equations were used to calculate the concentration of endogenous catecholamines in samples. All integrated peaks were checked for accuracy.

Human Flow cytometry

Tonsillar lymphocytes were stained with the following anti-human antibodies – CD4 APCy7 (RPA-T4, BD Biosciences), CXCR5 Alexa 488 or Alexa 647 (RF8B2, BD Biosciences), PD-1 PE (MIH4, eBioscience) or BV605 or BV421 (EH12.2H7, BioLegend), CD127 FITC (11-1278, eBioscience) or BV 421 (A019D5, BioLegend),

CD25 biotin (BC96, eBioscience or BioLegend) or PE-Cy7 (BC96, BD Biosciences or BioLegend), BCL6 Alexa 647 or PE-Cy7 (K112-91, BD Biosciences), CD3 APC (HIT3a, BD Biosciences) or Alexa 700 (UCHT1, BD Biosciences), CD27 FITC or APC (M-T271, BD Biosciences), CD38 FITC (HIT2, BD Biosciences) or PE (HB7, BD Biosciences), ICOSL APC (2D3, BioLegend), FAS PE-CF594 (DX2, BD Bioscience), CD40 APCCy7 (5C3, BioLegend), BAFFR PECy7 (11C1, BioLegend), CD19 PECy7 or BV605 (SJ25C1, BD Bioscience), IL21R BV421 (17A12, BioLegend), CD86 BV421 (2331/FUN-1, BD Bioscience). All surface stains were performed in the presence of Human TruStain FcX (cat. 422302, BD Bioscience). Intracellular staining was performed using the FOXP3/Transcription Factor Staining Buffer Set (eBioscience) according to the manufacturer's instructions. Cells were stained with primary antibodies followed by secondary reagents for 30 min at 4 °C. Data were collected on a LSRII or Fortessa cytometer (BD) and analysed with FlowJo software (TreeStar). 7-AAD (Invitrogen) or Zombie Aqua (BioLegend) staining was used to exclude dead cells from analysis.

Immunofluorescent and flow cytometric detection of dopamine

Freshly isolated human T_{FH} cells were stimulated with 10 µM forskolin (Sigma) for 24h in RPMI 1640 medium supplemented with 3% BSA, 50 µg/ml D-glucose (Sigma), 2 mM L-glutamine, 100 U penicillin-streptomycin, 0.1 mM non-essential amino acids and 100 mM Hepes (Gibco, Thermo Fisher Scientific). Cells were then collected, prefixed with 50 mM cacodylate and 1% sodium metabisulfite (MBS, Sigma) and fixed with 5% glutaraldehyde (GA) in 0.1 M cacodylate and 1% MBS for 15 min at RT. After washing with 1% MBS in 50 mM Tris (Tris-MBS) twice, the cells were incubated with or without rabbit anti-dopamine pAb (Millipore) in Tris-MBS containing 0.05% Triton-X for 1h at RT, followed by Alexa Fluor 488-conjugated anti-rabbit IgG (Invitrogen) for 30 min at RT. After washing with Tris-MBS, samples were mounted on cover glasses and visualized with a Zeiss Axio Observer microscope and then were analyzed with a LSR Fortessa (BD).

Dopamine release

Following 24 h stimulation with forskolin, as previously described, 1x10⁵ freshly isolated human T_{FH} cells were cultured with 1x10⁵ anti-CD3/CD28 beads, 2x10⁵ autologous or allogeneic CellTrace Violet (CTV, Thermo Fisher Scientific) labeled GC B cells for 30 min. After culture cells were fixed and stained for dopamine following the protocol described previously and analyzed with a LSR Fortessa (BD).

Dopamine in vitro stimulation

For short term stimulation, 2×10^5 sorted human GCB or 5×10^5 enriched B cells were stimulated for 30 min with $10 \mu\text{M}$ of freshly prepared DA (Sigma), 10 nM of dopamine receptor 1 agonist (SKF38393, Tocris), 10 nM of dopamine receptor 1 antagonist (SKF83566, Tocris) or 50 nM of Haloperidol (Tocris) in RPMI 1640 medium supplemented with 10% FCS, 2 mM L-glutamine, 100 U penicillin-streptomycin, 0.1 mM non-essential amino acids and 100 mM Hepes. Because Dopamine HCl (dopamine hydrochloride) is sensitive to alkalis, iron salts and oxidizing agents (i.e. light and air), solutions were always prepared from powder immediately before use. Cells were stained for ICOSL, CD40, CD86, FAS, IL21R, BAFFR, Zombie live-dead marker and intracellular Bcl6, and analysed on LSRII. For long term culture 2×10^5 sorted GC B cells were stimulated with a range of DA dilutions for 5 days and stained for 7-AAD, CD27, CD4, CD19 and CD38 and analysed on LSRII. For the experiment with dopamine receptor block, 2×10^5 sorted GC B cells were stimulated with $5 \mu\text{M}$ of freshly prepared DA with or without 50 nM of Haloperidol (Tocris) for 2 h. Incubation media was then replaced with fresh media containing anti-CD40 ($1 \mu\text{g/ml}$, BioLegend) and IL-21 (10 ng/ml , Peprotech), cells were incubated for 5 days and plasma cell differentiation was assessed.

RT- PCR analysis

Total RNA was isolated from freshly isolated T and B cell subsets ($n=5$) using trizol (Invitrogen), then transcribed into cDNA by MLVRT synthesis (Invitrogen) and used as a template for qPCR to assess CHGB (F, 5'-TGC CAG TGG ATA ACA GGA AC-3'; R, 5'-TCT TCA GGA CTT GGC GGC A-3')⁴ and DRDs (DRD1 F, 5'-CAG TCC ACG CCA AGA ATT GCC-3'; DRD1 R, 5'-ATT GCA CTC CTT GGA GAT GGA GCC-3'; DRD3 F, 5'- TGG ATG TCA TGA TGT GTA CAG CC-3'; DRD3 R, 5'- TCC CCT GTG GTA TTA AAG CCA AAC-3'; DRD5 F, 5'-GTC GCC GAG GTG GCC GGT TAC-3'; DRD5 R, 5'-GCT GGA GTC AGA ATT CTC TGC AT-3')⁵ expression. To evaluate changes in the expression of CHGB and TH (F, 5'- TGT GAA GGT GTT TGA GAC GTT TG-3'; R, 5'-TCG AGG CGC ACG AAG TAC T-3'), total RNA was isolated from T_{FH} cells after 24 h forskolin treatment. $\beta 2$ -microglobulin (F, 5'-TGC TGT CTC CAT GTT TGA TGT ATC T-3'; R, 5'-TCT CTG CTC CCC ACC TCT AAG T-3') or RPL13A (F, 5'-CCT GGA GGA GAA GAG GAA AGA GA-3'; R, 5'-TTG AGG ACC TCT GTG TAT TTG TCA A-3') have been used as housekeeping gene. Mouse CHGB expression was evaluated using a TaqMan based assay (CHGB, Mm00483287_m1;

GAPDH, Mm99999915_g1). The relative expression was calculated using the 2^{-ddct} method⁶.

RNA sequencing

Human follicular T helper, follicular T regulatory, T naive cells, memory and GC B cells were FACS purified from 3 fresh tonsils. Memory and GC B cells were stimulated with 5 μ M of freshly prepared DA in complete RPMI 1640 for 2 h. mRNA was then extracted and sent to the ACRF Biomolecular Resource Facility, The John Curtin School of Medical Research, Australian National University for library construction using the TruSeq Stranded mRNA LT Sample Prep Kit (Illumina). Library samples were sequenced on a HiSeq2000 with a coverage of 25 million reads. The data was then sent to the Genome Discovery Unit (ANU Bioinformatics Consulting Unit, JCSMR, ANU) for analysis. There were a total of 621,384,768 raw 100bp paired-end reads from the sequencer across 18 samples and two lanes. Initial quality control checks were performed using FastQC and reads were subsequently trimmed using Trimmomatic⁷ version 0.32 with conservative settings (LEADING:15 TRAILING:15 SLIDINGWINDOW:4:20 MINLEN:60) which retained 506,390,951 high-quality read pairs (81.5%). All reads were aligned to the *H. sapiens* genome reference sequence using TopHat version 2.0.13 with default parameters. Read counts were then generated for each gene in each sample using featureCounts version 1.4.6-p1 by using annotated gene locations. Differential expression analysis was performed using the edgeR package version 3.10. Read counts per gene were normalized by trimmed mean of M-values (TMM). As edgeR uses the negative binomial distribution as its basic model for differential expression data, dispersion estimates are obtained using the quantile-adjusted conditional maximum likelihood (qCML) method for single factor experiments. Then, the qCML-based exact test for the negative binomial distribution was performed to test for differentially expressed genes in our groups of samples. We used a Benjamini-Hochberg adjusted p-value threshold of 0.05 to identify significantly differentially regulated genes.

Live RNA detection

Freshly isolated human tonsil cells were also used for transfection experiments with SmartFlareTM RNA detection probes (Millipore) specific for CHGB (5'-CCCAGCTTAGAGCTTGATAAGATGGCA-3'). 5×10^4 cells/well were treated with 4 μ L diluted probe (1:20 in sterile PBS) and incubated overnight (16 h) at 37°C in an atmosphere of 5% CO₂. In each experiment, two controls were included: a scramble SmartFlareTM Probe, which does not recognize any cellular sequence and served as

a control to determine the background; an uptake SmartFlare™ Probe, which permanently fluoresces and provided the information that the SmartFlare™ particles were incorporated by the target cell type. Cells were stained for CD3, CD4, CXCR5, CD19, PD-1, CD45RO and DAPI (as live-dead marker). Fluorescence was evaluated using a LSR Fortessa flow cytometer.

Supported Lipid Bilayer (SLB) and TIRFM Imaging

SLB were formed as previously described^{8,9}. Briefly, glass coverslips were cleaned with 70% H₂SO₄/30%H₂O₂, rinsed extensively, dried, and assembled into disposable 6 channel chambers (Ibidi). SLB were formed by incubation of each channel with small unilamellar vesicles containing 12.5 mol% 1,2-dioleoyl-*sn*-glycero-3-[(N-(5-amino-1-carboxypentyl) iminodiacetic acid) succinyl] (nickel salt) and 0.05 mol% 1,2-dioleoyl-*sn*-glycero-3-phosphoethanolamine-N-(cap biotinyl) (sodium salt) in 1,2-dioleoyl-*sn*-glycero-3-phosphocholine at total phospholipid concentration 0.4 mM. Chambers were flooded with human serum albumin (HSA)-supplemented HEPES buffered saline (HBS), subsequently referred to as HBS/HSA. Following blocking with 5% casein in PBS containing 100 µM NiSO₄, to saturate NTA sites, unlabelled streptavidin was then coupled to biotin head groups. Biotinylated UCHT1 (10 molecules/µm²) and His-tagged ICAM-1 (200 molecules/µm²), CD40 (300 molecules/µm²) and ICOSL (200 molecules/µm²) were then incubated with the bilayers at concentrations to achieve the indicated site densities. Anti-CD3/CD28 Dynabead stimulated CD4⁺ T cells (day 7) were suspended in HBS/HSA and labelled with 5 µg/mL Alexa Fluor 488 anti-CD40L antibody prior to incubation with the bilayers at 37°C for 15 minutes. Cells were then fixed at room temperature for 10 minutes with 2% formaldehyde in PHEM buffer. For experiments involving T_{FH} cells frozen tonsil cell suspension was enriched for T cells (EasySep negative selection, Stemcell) and sorted on CXCR5^{hi} and CXCR5^{low}. Following synapse formation of 20 minutes the cells were fixed in 2% PFA in PHEM buffer for 10 minutes at RT and permeabilised with 0.1% Triton X-100 in HBS/HSA. Cells were then blocked with 5% Casein containing 5% Donkey serum for 1hour, washed with HBS/HSA and stained with anti-CgB in 5% Casein overnight. Followed by a secondary antibody in 5% Casein containing 5% Donkey serum for 60 minutes. Imaging was done on an Olympus IX83 inverted microscope equipped with a TIRF module. The instrument was fitted with an Olympus UApON 150x TIRF N.A 1.45 objective, 405 nm, 488 nm, 568 nm and 640 nm laser lines and Photomertrics Evolve delta EMCCD camera.

Score for CD40L and CgB intensity and ICAM-1 positive area was conducted on blinded images.

Modelling the effect of Dopamine on GC reaction

In view of restrictions to test the impact of fast and slow signalling in GC-B cells in humans, we employed mathematical modelling to speculate on possible implications. Predictions from mathematical models bear the risk of relying on particular assumptions. We therefore repeated the analysis in different models and only accepted the results consistently reproduced in all models.

At first, we used the current state-of-the-art model of the GC reaction¹⁰⁻¹² to investigate the impact of fast versus slow acquisition of help signals from T_{FH} to B cells. The interaction time of B and T cells was set to 36 min and 4 h, to mimic the fast dopamine dependent ICOSL upregulation versus the slow dopamine-independent ICOSL upregulation. In order to make GC simulations comparable, the required duration of T_{FH} signalling to B cells was adapted from 0.5 to 1.5 h. Longer T-B-interactions induced reduced output while keeping affinity maturation unchanged (Fig. S7, black curves for fast and red curves for slow ICOSL upregulation). Note that the GC strength (Ω), defined as the area under the curve of the GC B cell population kinetics¹⁰, was comparable in both simulations (Fig. S7, legend box), such that the effect on output production is not simply reflecting smaller GC sizes.

This result might rely on the secondary effect on the DZ to LZ ratio. To exclude this explanation for the observed reduced output, simulations with long T-B-interactions were retuned to match GC strength and DZ to LZ ratio between simulations with short and long T-B-interactions. Comparable GC volume and GC strength as well as the physiological DZ to LZ ratio were restored in silico by adapting three parameters: (i) the amount of collected antigen at which T_{FH} induce half maximum numbers of divisions in selected B cells (K_D), (ii) the duration of signalling by T_{FH} required for B cell selection (ΔT_{min}), and (iii) the amount of antigen presented per follicular dendritic cells (Ag_{FDC}). The result that output production is reduced in simulations with longer T-B-interactions while keeping affinity maturation unchanged was confirmed in all settings (Fig. S7, black curves for fast and coloured curves for slow ICOSL upregulation, non-red curves with GC strength correction). By variation of the model parameters, we were not able to find a simulation in which longer T-B-interaction would not reduce output production.

In vivo, B cells integrate signals from many short contacts of 5 minutes to T_{FH} cells¹³. The phenomenological representation of this signal-integration by a single interaction between T_{FH} and GC-B cells in silico might be considered as a limitation of the previous approach. We therefore extended the mathematical model to better reflect the in vivo situation. Each instance of the B cell class was extended by a variable representing the amount of T_{FH} signals received and by a variable representing the degree of ICOSL upregulation. B cells search for T_{FH} help for a period derived from the amount of antigen they collected from FDCs. In this period (Δt_{Th}), they interact with different T_{FH} for 5 minutes each. As in the old model, T_{FH} polarise towards the B cell which presents most pMHC in the case that more than one B cell attempts to get signals from the same T_{FH} . The amount of signals received by a B cell in each interaction with a T_{FH} is assumed to be proportional to the duration of T_{FH} polarisation towards the B cell multiplied by the ICOSL level (fraction of max expression) of the B cell. This latter assumption reflects the positive feedback loop between ICOS and CD40 signalling in T-B-interactions¹⁴. The amount of integrated signal determines the number of divisions that is attributed to the B cell in the next round of recycling^{10,15}. The number of divisions is calculated from the integrated signal with a Hill-function with Hill-coefficient 2 and characterised by the amount of signal required to induce two divisions ($S(N_p=2)$). Note that the number of divisions was derived from the amount of collected antigen in the previous version of the model. In this new model, fast and slow ICOSL upregulation is directly represented by shifting the K-value (Δt_{ICOSL}) of a Hill-function describing ICOSL upregulation over time. The level of ICOSL at any time impacts on the signalling strength in T-B-interactions (and by this on the number of B cell divisions) rather than on the duration of T-B-interactions (as in the previous model).

Despite a different selection model and a different impact point of the speed of ICOSL upregulation, the result that the production of output cells is retarded and reduced in simulations with slow ICOSL upregulation was confirmed (Fig. S8, black lines for fast versus green and red lines for slow ICOSL upregulation; grey lines for fast versus magenta lines for slow ICOSL upregulation). This also holds true, when the lower GC strength in simulations with slow ICOSL upregulation (Fig. S8, red lines) was compensated by a longer phase of search for T_{FH} help leading to higher numbers of divisions attributed to B cells (Fig. S8, orange lines).

While there was no impact on affinity maturation in GC-B cells (Fig. S8), the fewer output cells generated exhibited a consistently higher affinity (Fig. S8, all coloured lines show higher affinity than black or grey lines). Even though we consider the new model as more realistic, we excluded the impact on output affinity from the presentation in the main text, as it was not observed in all model variants.

The effect of slow ICOSL dynamics on speed and amount of output was reduced but persisted when a memory for ICOSL upregulation was assumed (Fig. S8, blue lines). In this setting, a selected B cell with upregulated ICOSL is thought to return to the DZ for further rounds of division. The dilution of ICOSL expression and of its mRNA onto the daughters is ignored (thus, overestimating memory) and all daughters, which restart search for T_{FH} help in the next round of selection, are assumed to keep full ICOSL competence. Even under this extreme and unrealistic condition, the effect on output production is kept, but less pronounced.

As the main impact point of the speed of ICOSL upregulation concerned output production we asked whether this result would depend on the choice of the output differentiation model. In the LEDA model, B cells that passed selection always return to the DZ and divide before they leave through the DZ. In the classical textbook GC, a subset of B cells that passed selection directly differentiates to output cells and leave the GC through the LZ. Both models lead to the same result (Figure S9), such that we conclude that the particular choice of how B cells differentiate to output cells and leave the GC is not at the origin of the dependence of output production on the speed of ICOSL upregulation.

What is the reason for less and slower output in simulations with slow ICOSL upregulation? The number of generated output cells depends on the GC size which is reduced by slow ICOSL upregulation. But less output is also observed in simulations in which the GC size was compensated. Note that the number of generated output cells is proportional to the number of B cell selection events. By slow ICOSL upregulation, the average level of ICOSL is lower in B cells. As a consequence, the amount of T_{FH} signals collected by B cells is reduced in silico which is supported by experimental data showing that ICOS signalling is part of a positive feedback loop in T-B-interactions¹⁴. This implies a stronger selection pressure and less selection events with slow ICOSL upregulation. In simulations with compensated GC size, the number of induced divisions in those B cells, which still passed selection, is higher (data not shown). The diversification of B cell receptors by

mutation, which more likely induce bad than good mutations, compensates the gain in affinity maturation induced by the higher selection pressure. This induces three effects by slow ICOSL upregulation:

- GC B cells have the same affinity maturation, which is the result of two concurring effects: higher selection pressure and higher B cell receptor diversification.
- The number of selection events is reduced, which leads to less output cells being generated by the same total number of GC B cells.
- The affinity of output cells is enhanced, because these are derived from a successful selection event with strong selection pressure before further diversification.

This explanation of the impact of the speed of ICOSL upregulation on output production is rather generic and involves the network of interactions active in GC reactions.

Each curve in Figures S7-S9 shows the mean and standard deviation of 100 independent simulations. Simulations were programmed in C++ and performed under Linux Ubuntu on Xeon E5 2690 v3 CPUs. Visualisation was done with the GLE software package.

Statistical Analysis

All data were analysed with two tailed non-parametric Mann-Whitney test (U test) except for ICOSL induction and DA in vitro stimulation experiments, in which two tailed unpaired Student's t test was used. Statistical tests with appropriate underlying assumptions on data distribution and variance characteristics were used. All statistical analysis was performed with Prism software (version 6, GraphPad Software). Statistically significant differences are indicated as * $p \leq 0.05$, ** $p \leq 0.01$, and *** $p \leq 0.001$; **** $p \leq 0.0001$ and ns = not significant.

References

- 1 Glass, G., Papin, J. A. & Mandell, J. W. SIMPLE: a sequential immunoperoxidase labeling and erasing method. *The journal of histochemistry and cytochemistry : official journal of the Histochemistry Society* **57**, 899-905, doi:10.1369/jhc.2009.953612 (2009).
- 2 Villa, A. *et al.* The endoplasmic-sarcoplasmic reticulum of smooth muscle: immunocytochemistry of vas deferens fibers reveals specialized subcompartments differently equipped for the control of Ca²⁺ homeostasis. *The Journal of cell biology* **121**, 1041-1051 (1993).
- 3 Smythe, G. A., Edwards, G., Graham, P. & Lazarus, L. Biochemical diagnosis of pheochromocytoma by simultaneous measurement of urinary excretion of epinephrine and norepinephrine. *Clinical chemistry* **38**, 486-492 (1992).
- 4 Slater, E. P. *et al.* Analysis by cDNA microarrays of gene expression patterns of human adrenocortical tumors. *European journal of endocrinology / European Federation of Endocrine Societies* **154**, 587-598, doi:10.1530/eje.1.02116 (2006).
- 5 Meredith, E. J. *et al.* Dopamine targets cycling B cells independent of receptors/transporter for oxidative attack: Implications for non-Hodgkin's lymphoma. *Proceedings of the National Academy of Sciences of the United States of America* **103**, 13485-13490, doi:10.1073/pnas.0605993103 (2006).
- 6 Livak, K. J. & Schmittgen, T. D. Analysis of relative gene expression data using real-time quantitative PCR and the 2(-Delta Delta C(T)) Method. *Methods* **25**, 402-408, doi:10.1006/meth.2001.1262 (2001).
- 7 Bolger, A. M., Lohse, M. & Usadel, B. Trimmomatic: a flexible trimmer for Illumina sequence data. *Bioinformatics* **30**, 2114-2120, doi:10.1093/bioinformatics/btu170 (2014).
- 8 Dustin, M. L., Starr, T., Varma, R. & Thomas, V. K. Supported planar bilayers for study of the immunological synapse. *Current protocols in immunology / edited by John E. Coligan ... [et al.] Chapter 18*, Unit 18 13, doi:10.1002/0471142735.im1813s76 (2007).
- 9 Choudhuri, K. *et al.* Polarized release of T-cell-receptor-enriched microvesicles at the immunological synapse. *Nature* **507**, 118-123, doi:10.1038/nature12951 (2014).
- 10 Meyer-Hermann, M. Overcoming the dichotomy of quantity and quality in antibody responses. *Journal of immunology* **193**, 5414-5419, doi:10.4049/jimmunol.1401828 (2014).
- 11 Meyer-Hermann, M. *et al.* A theory of germinal center B cell selection, division, and exit. *Cell reports* **2**, 162-174, doi:10.1016/j.celrep.2012.05.010 (2012).
- 12 Tas, J. M. *et al.* Visualizing antibody affinity maturation in germinal centers. *Science* **351**, 1048-1054, doi:10.1126/science.aad3439 (2016).
- 13 Allen, C. D., Okada, T., Tang, H. L. & Cyster, J. G. Imaging of germinal center selection events during affinity maturation. *Science* **315**, 528-531, doi:10.1126/science.1136736 (2007).
- 14 Liu, D. *et al.* T-B-cell entanglement and ICOSL-driven feed-forward regulation of germinal centre reaction. *Nature* **517**, 214-218, doi:10.1038/nature13803 (2015).
- 15 Gitlin, A. D., Shulman, Z. & Nussenzweig, M. C. Clonal selection in the germinal centre by regulated proliferation and hypermutation. *Nature* **509**, 637-640, doi:10.1038/nature13300 (2014).

Fig. 1

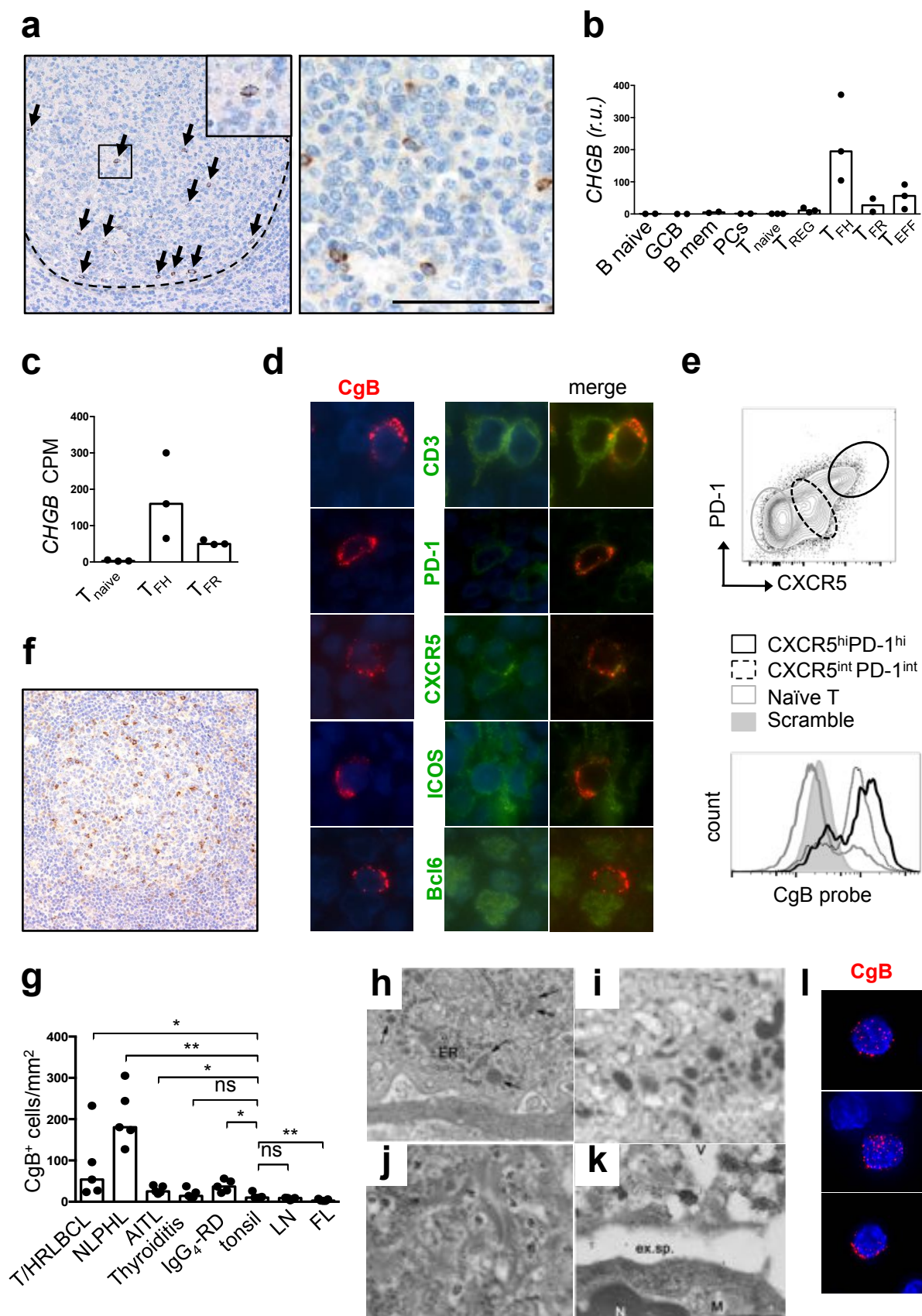


Fig. 2

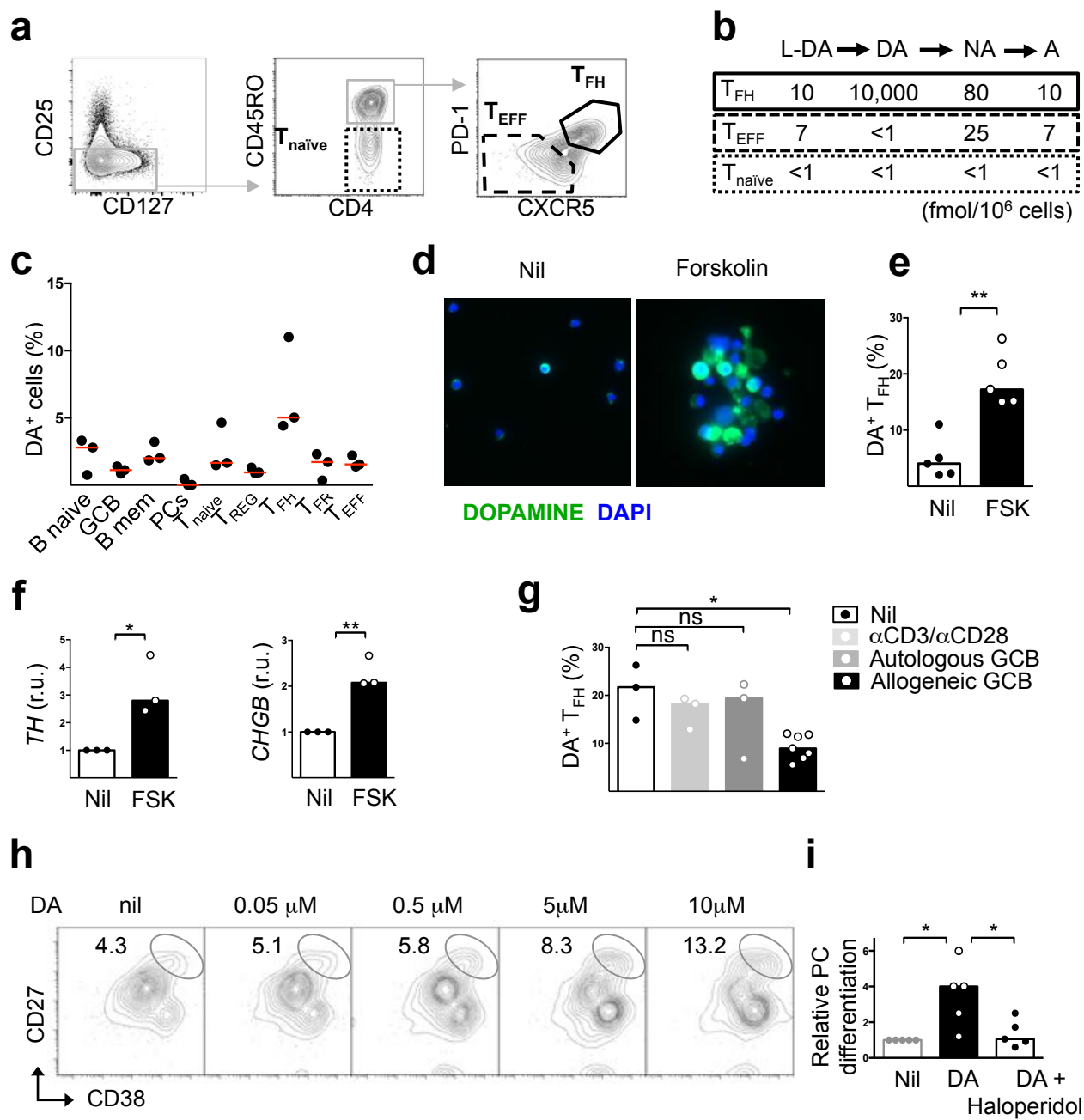


Fig. 3

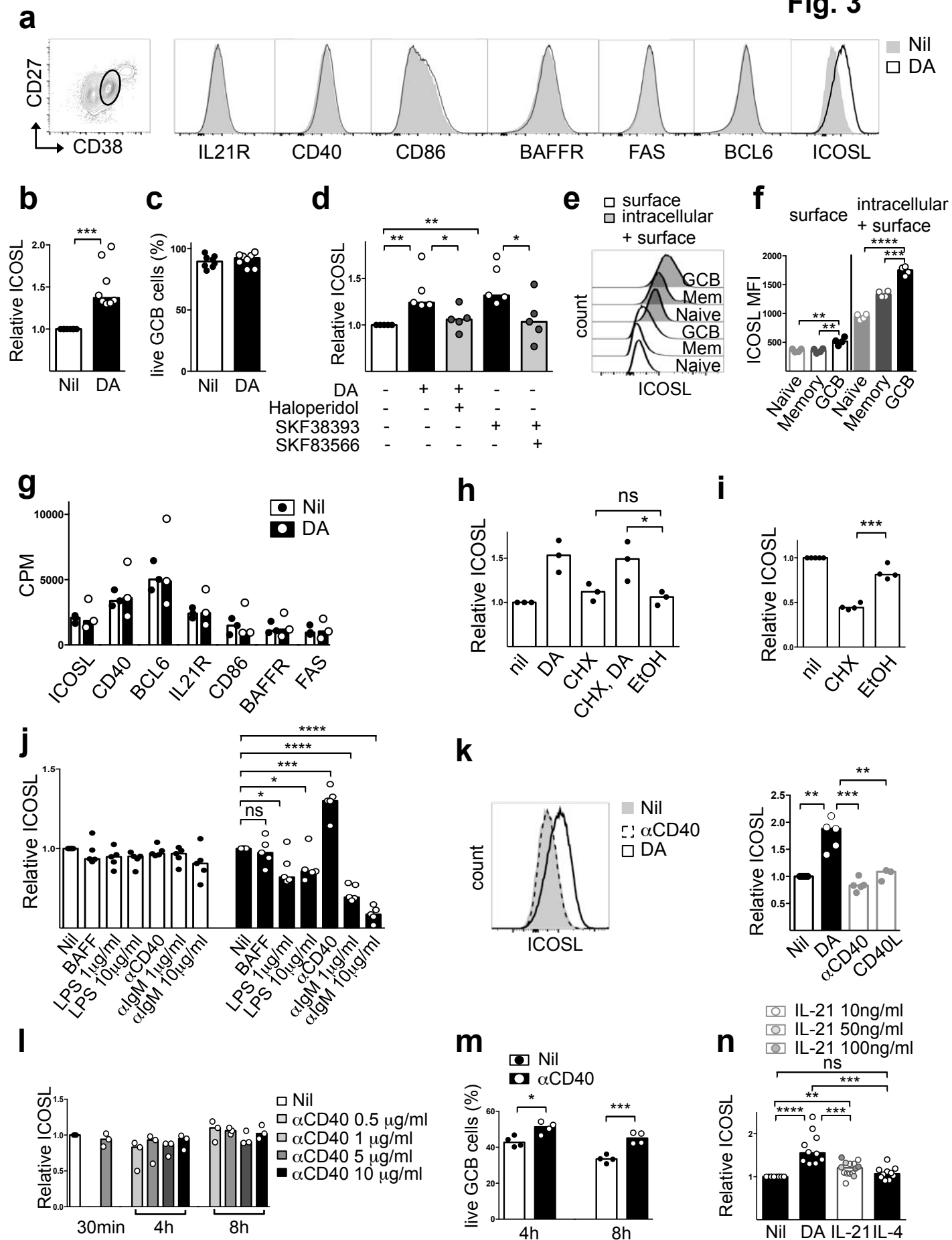


Fig. 4

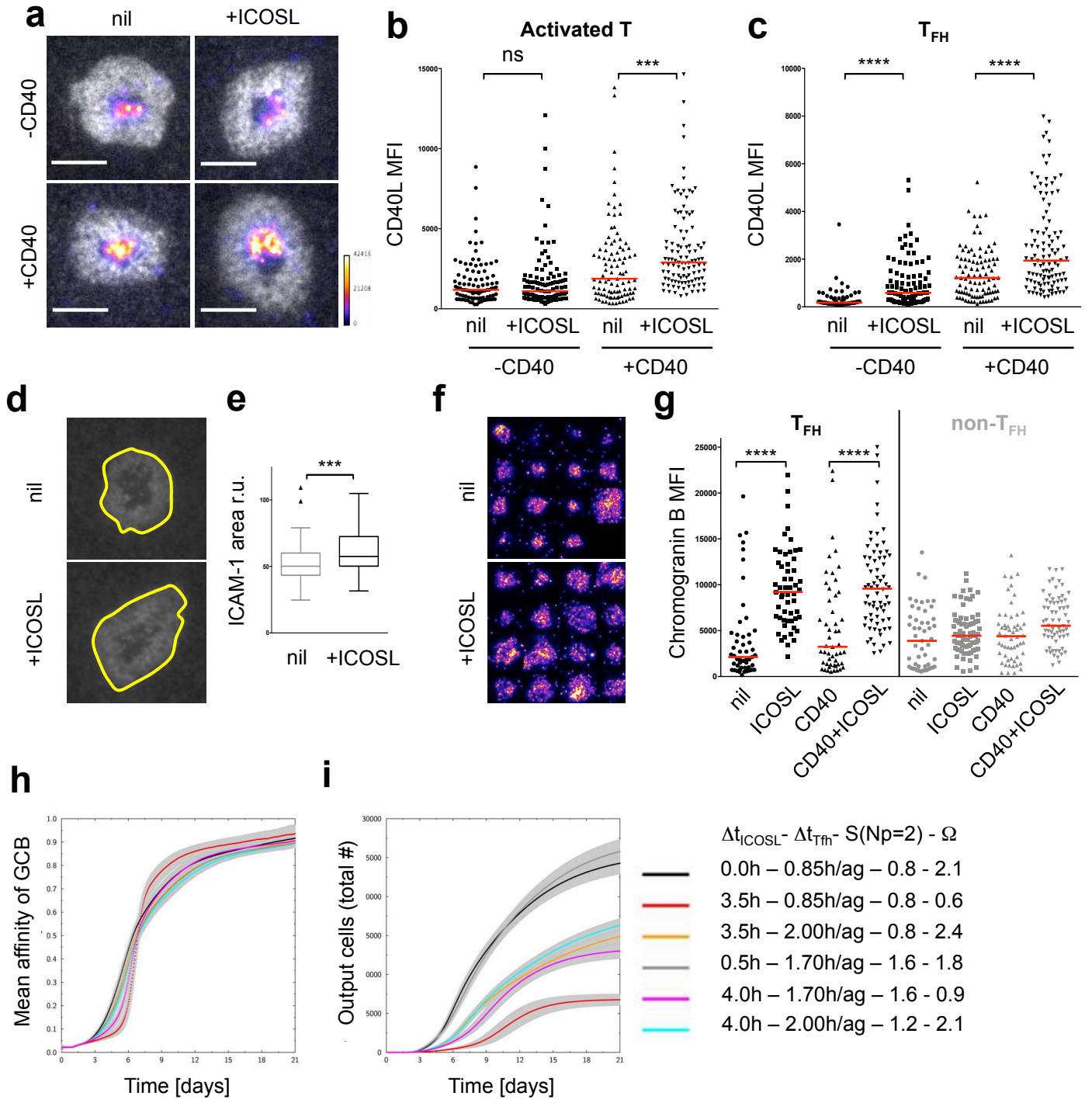


Fig. S1

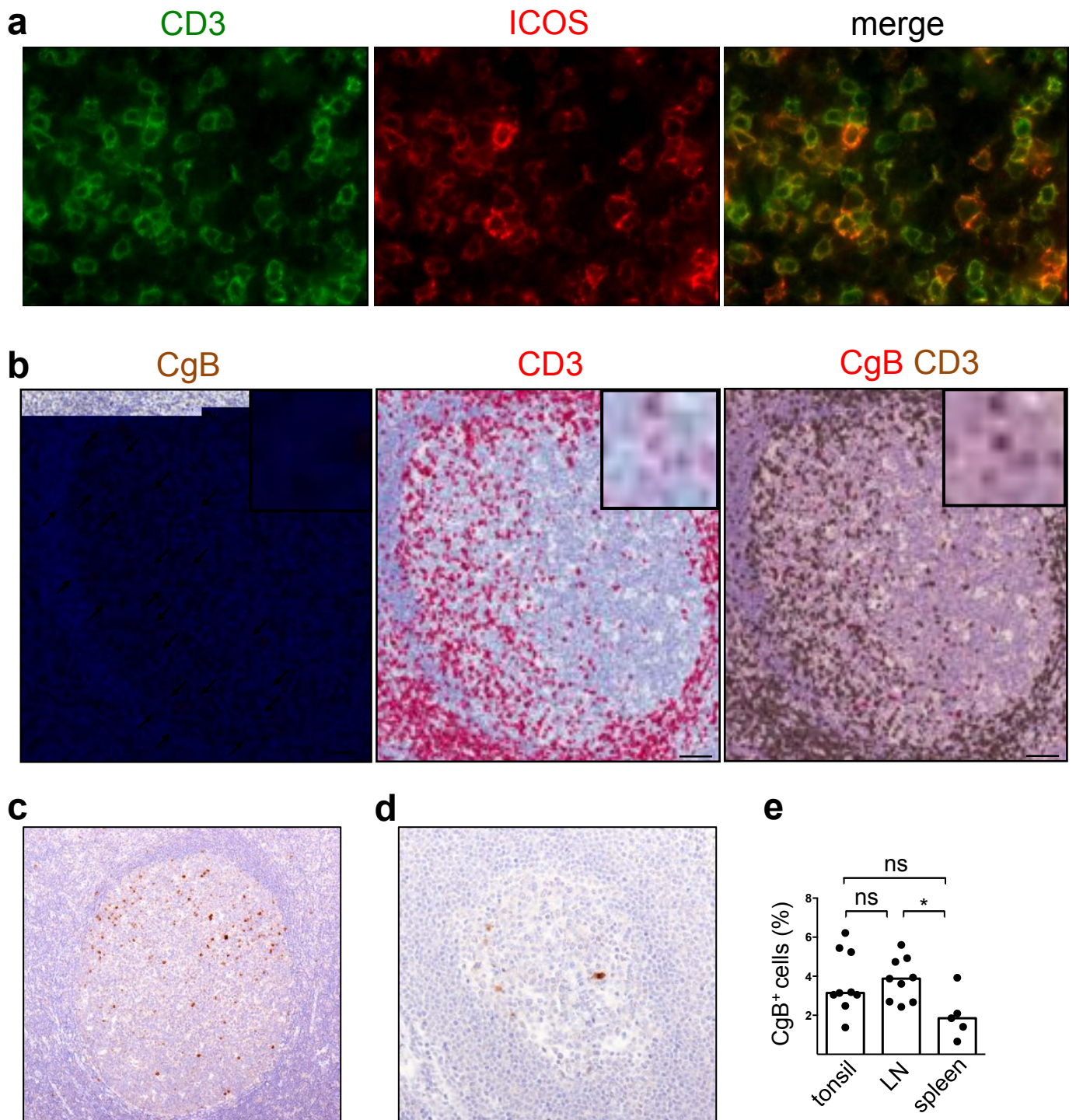


Fig. S2

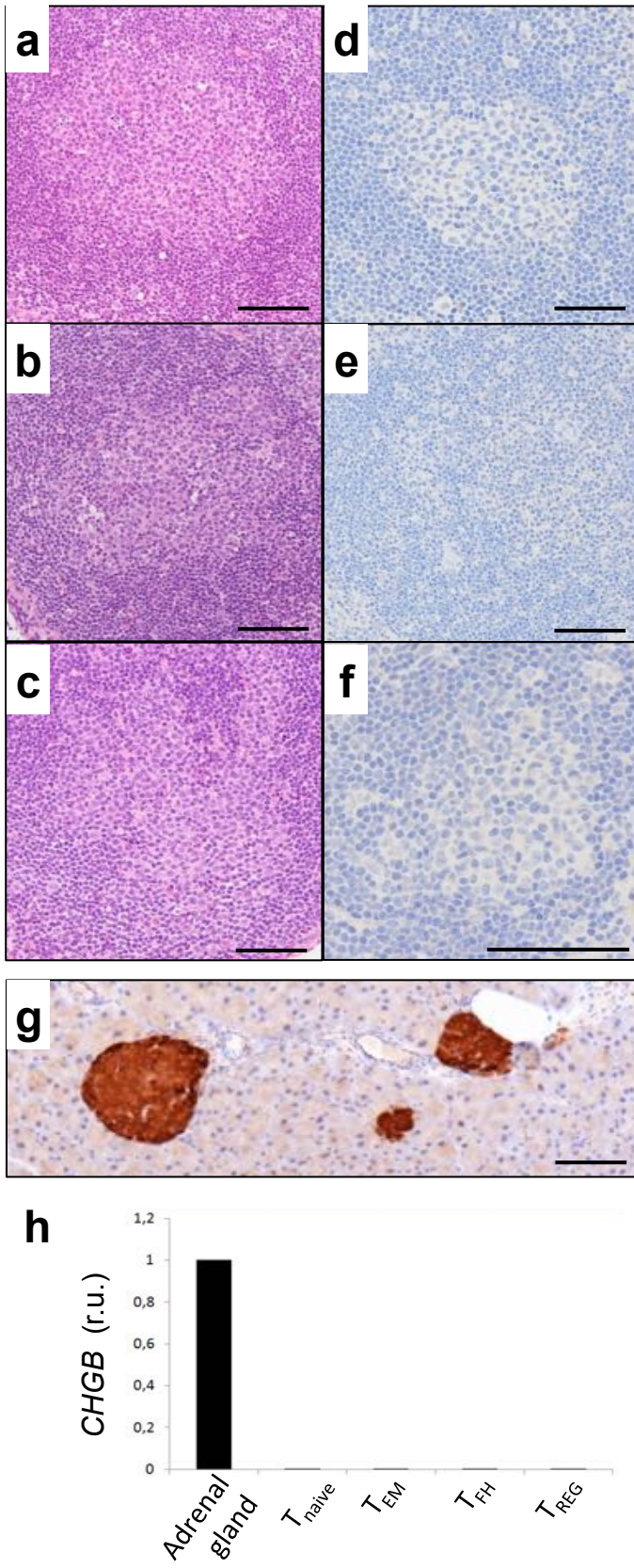


Fig. S3

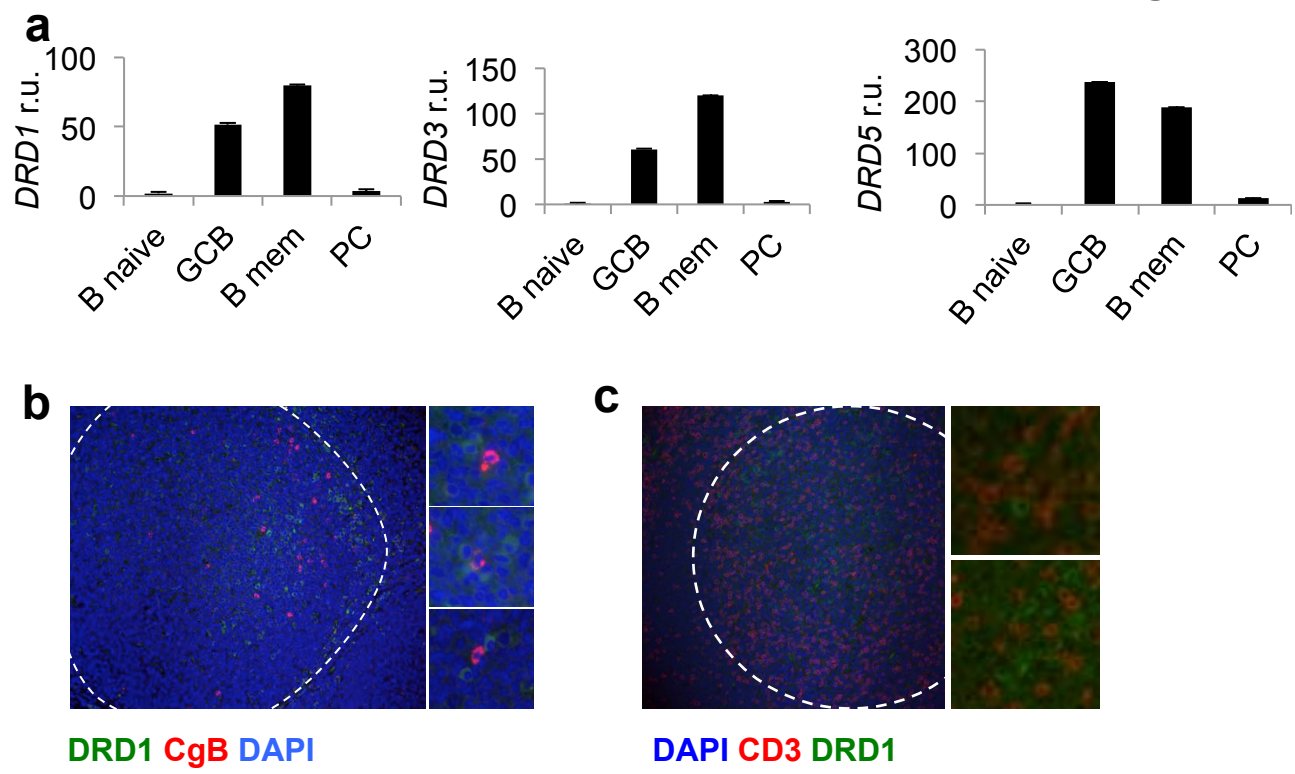


Fig. S4

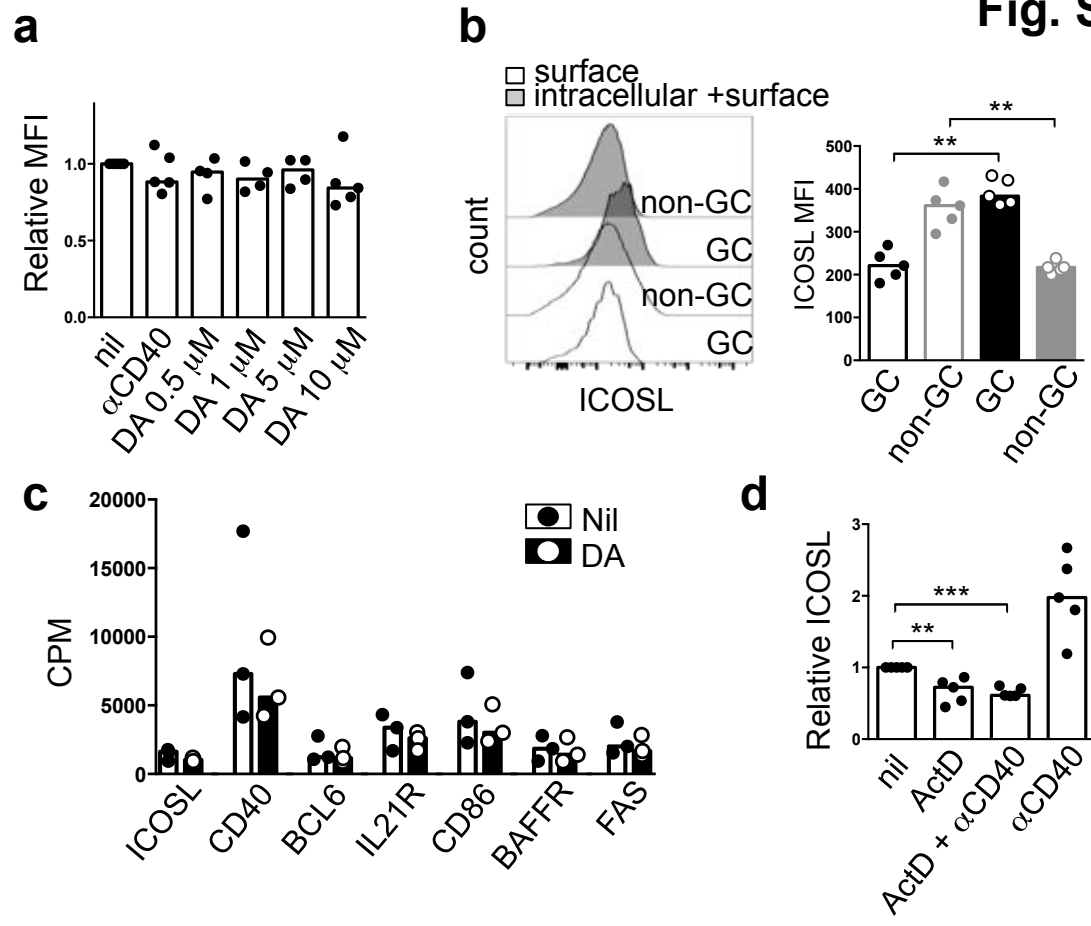
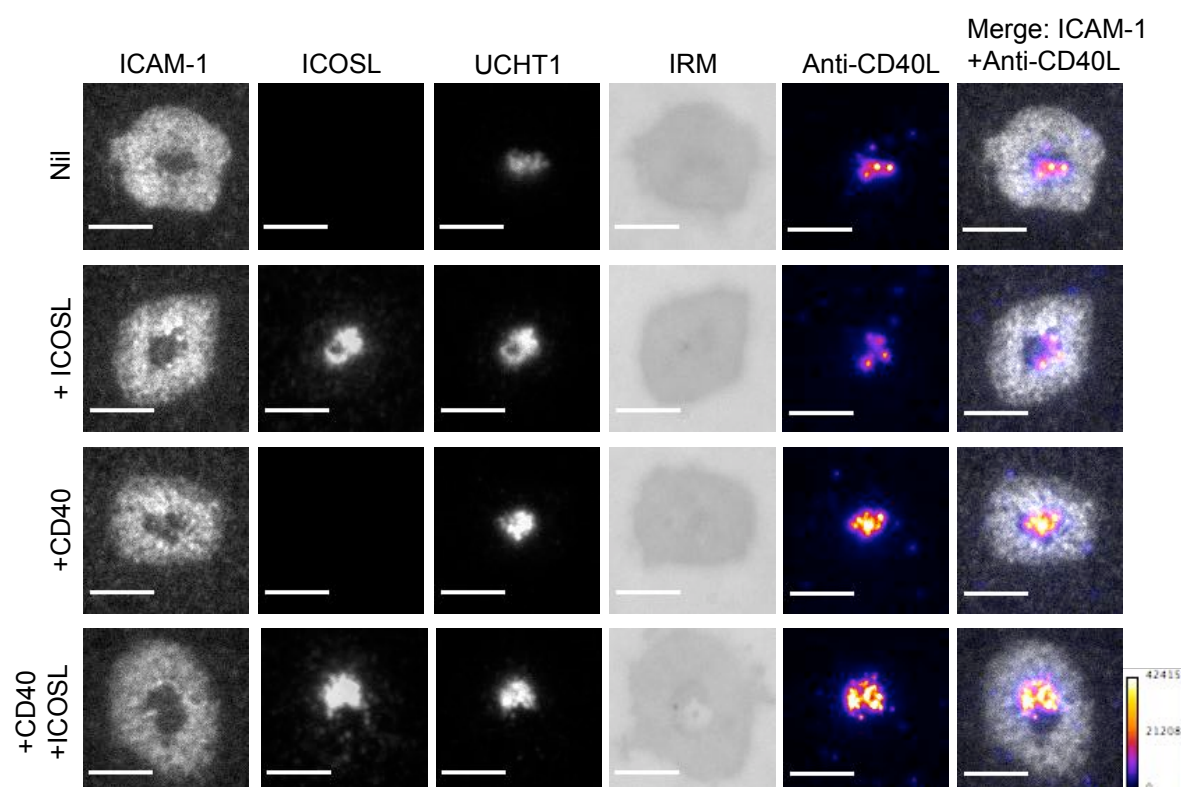


Fig. S5

a



b

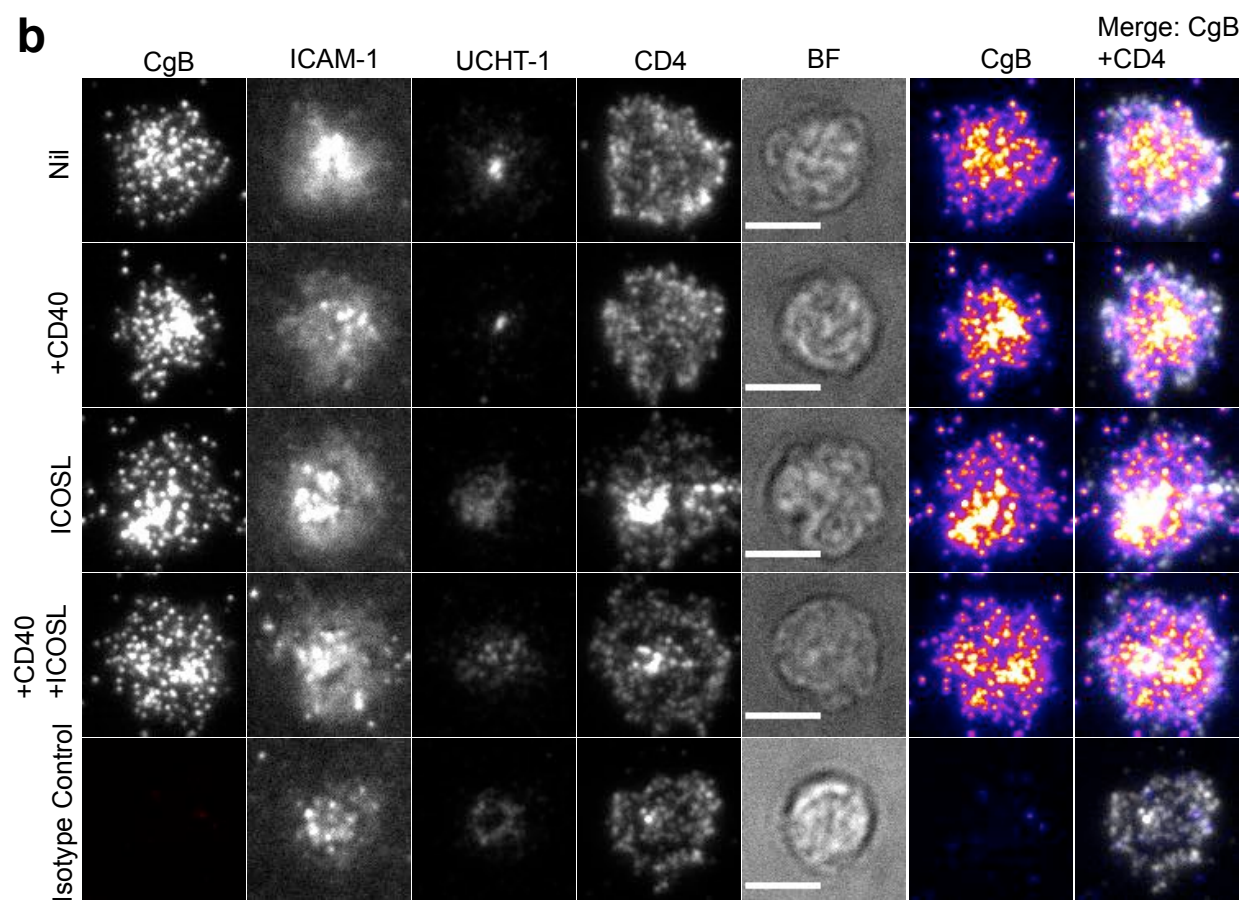


Fig. S6

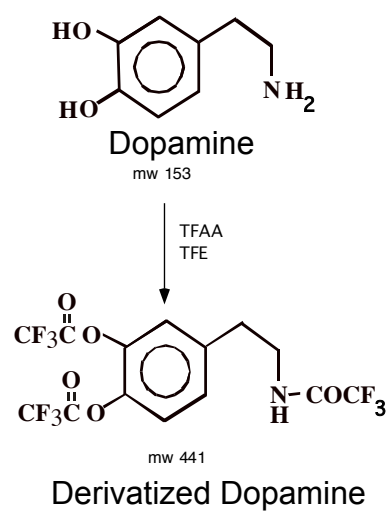


Fig. S7

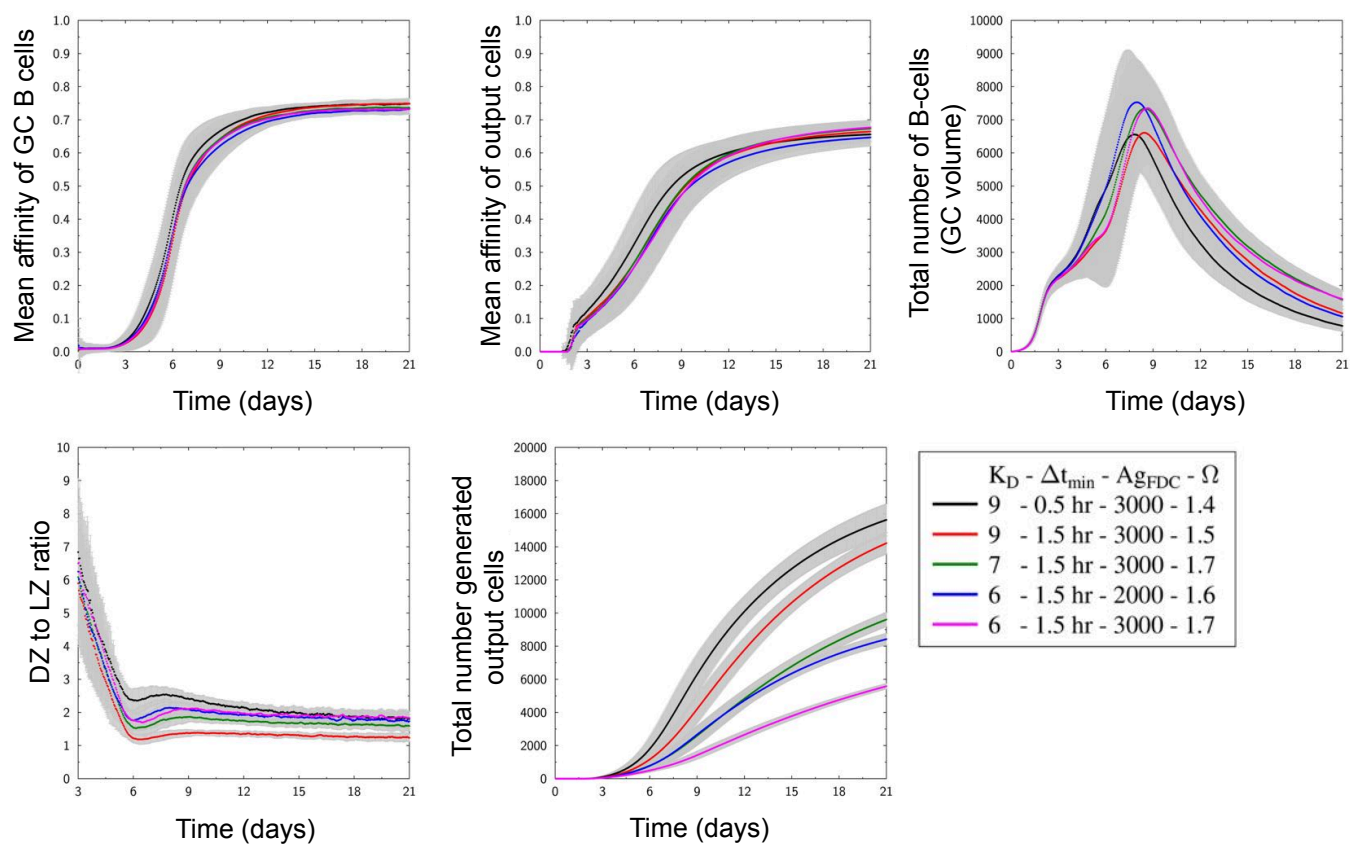


Fig. S8

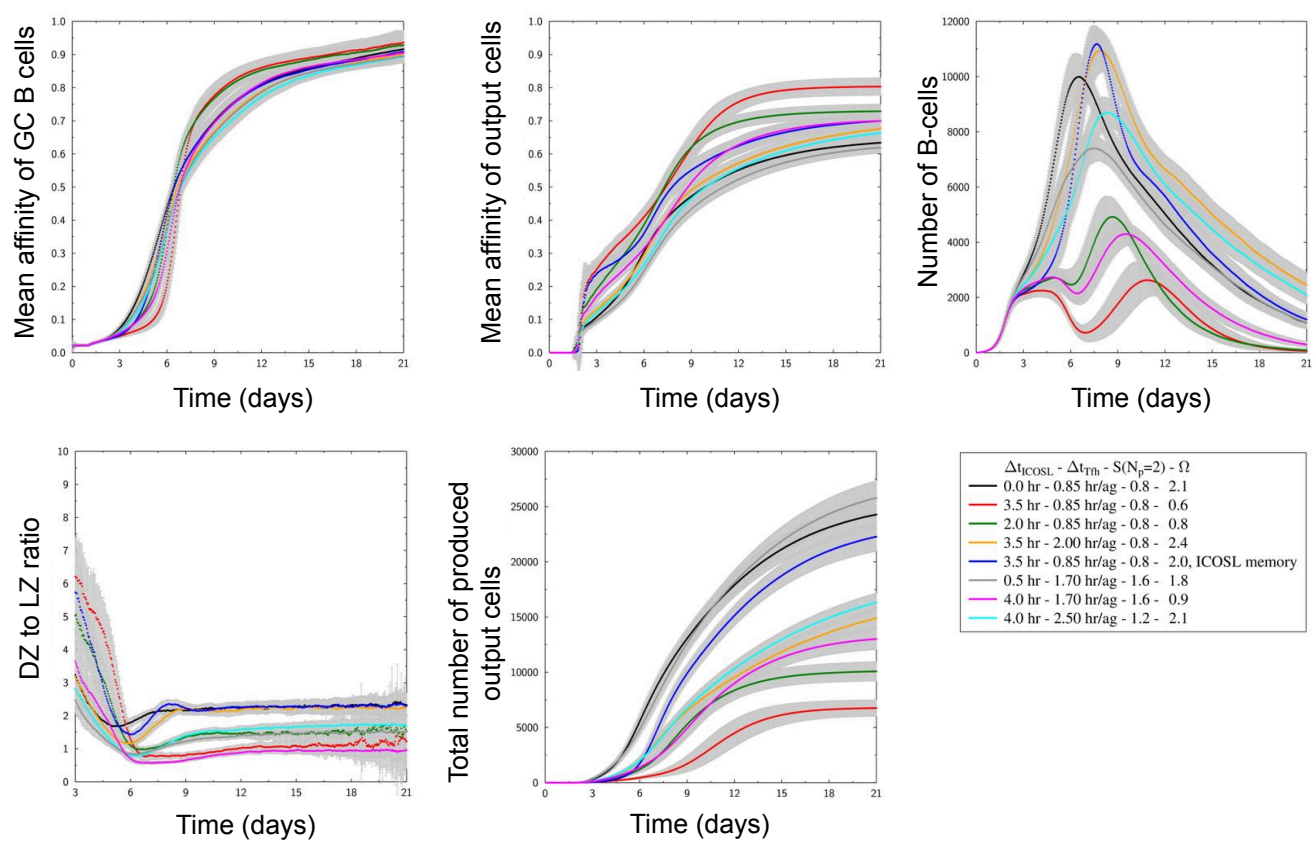


Fig. S9

